Hochschule für Angewandte Wissenschaften Hamburg
Hamburg University of Applied Sciences

Universitätsklinikum Hamburg-Eppendorf

Master Thesis

Simulation and Measurement of Fetal Blood Oxygen Saturation based on T2 Values at 3T MRI

Author: Rosa Elena Ortiz Reyes

HAW Examiner (1): Prof. Dr. Ing. Friedrich Ueberle

UKE Supervisor (2): M.Sc. Christian Ruprecht

Start Date: 13/03/2017

I hereby confirm that I am the author of the Master Thesis presented. I have written the Master Thesis as applied for previously unassisted by others, using only the sources and references stated in the text.

Hamburg August 30, 2017 Rosa Elena Ortiz Reyes

1 Abstract

Objective:

Recent studies have proven a dependency between MRI relaxation times ($T2^*$, $T2$) and blood oxygen saturation levels (sO_2) applying blood oxygenation level dependent (BOLD) sequences [24, 27, 49]. With this approach, the present work focuses on measuring the $T2$ dependency on fetal sO_2 at 3T MRI in-vitro and quantifying its relationship. Thereafter this quantification would be applied to in-vivo fetal imaging to develop a non-invasive method that measures sO_2 based on signal intensities.

Method: $T2$ measurements were performed on a 3T MRI scanner using a $T2$ preparation pulse and a balanced- SSFP sequence. Calibration experiments where made using $MnCl_2$ phantoms and hole blood samples retrieved from the umbilical cord. Signal intensities where fitted by a monoexponential equation to calculate $T2$ values, and a quadratic model was applied to determine the oxygen dependency. Afterwards, signal intensities in the fetal left ventricle where obtained in-vivo and correlated with the in-vitro calibration.

Results: The resulting quantitative correlation equation used for calculating fetal oxygenation in-vivo is $R2 = 0.0041 + 0.058(1-x) - 0.033(1-x)^2$. By this means, a 64% sO_2 for the left ventricle in fetal heart was calculated from in-vitro parameters.

Conclusion: The achieved results yield a clear relationship between $T2$ and sO_2 obtained by a blood oxygen level dependent sequence (BOLD), thus demonstrating that a non-invasive estimation of fetal oxygenation is feasible through an in-vitro calibration method. The quantification of this dependency is expected to support the use of BOLD for fetal blood oxygenation measurements in the future, facilitating the detection of abnormal oxygen supply in the gestational period.

Contents

2 Introduction

2.1 Motivation

The embryonic development and stem cell differentiation are directly dependent on the oxygen availability during the gestation period, where it acts as a key regulator of essential processes such as angiogenesis, haematopoiesis, and cardiogenesis [22, 29, 43]. Moreover, gas exchange between mother and fetus through the umbilical cord is considered one of the main influential factors of fetal development since the fetal lungs are inactive inside the womb [43].

In contrast, persistent exposure of the fetus to an hypoxic environment has a negative impact on fetal growth and abnormal placenta development. The consequences of this oxygen deprivation could lead to asphyxia, multi-organ failure, premature delivery, and even perinatal death. [45].

According to a World Health Organization demographic study in 2008, over 2.6 million perinatal deaths occur worldwide per year and 26% of these are attributed to intrauterine hypoxia [52]. This mortality rate could be reduced by early detection of low oxygen levels during the gestation period.

The current techniques for detecting fetal hypoxia narrow down to:

- **Doppler ultrasound velocimetry:** It assesses the blood flow in fetal vascularity, but does not calculate directly blood oxygen saturation values. This method can detect flow decrements in the umbilical artery, which indicate an increment in placental resistance and the need of further analysis. [34].
- **Percutaneous umbilical blood sampling:** Obtained trans-abdominally under ultrasound guidance by needle puncture of the umbilical cord. Because of its invasive nature, the associative risks are greater than in other tests, with a fetal death incidence of 2%. [13].

Recent studies have proven a direct dependency between relaxation times of blood and the oxygen contained in the hemoglobin molecules. According to those studies it is feasible to determine fetal blood oxygen saturation levels (sO_2) using either a $T2$ or $T2^*$ weighted MRI sequence [24, 27, 33, 49, 53]. With this approach, the development of a non-invasive method that estimates fetal sO_2 levels prepartum would provide the means to detect abnormal fetal oxygen supply and prevent their consequences.

The present work focuses on measuring the $T2$ value dependency on fetal blood oxygenation in-vitro at 3T MRI and quantify their relationship. This quantification would then be applied to in-vivo fetal imaging for estimating the sO_2 values in a non-invasive manner.

2.2 Project goals

Develop a method for measuring fetal oxygen saturation levels in a direct and non-invasive manner by detecting $T2$ relaxation values in MRI 3T.

2.2.1 Deliverables

- Parametric model of $T2$ values correlated with blood oxygen saturation.
- Data generated for model verification.
- Fetal phantom simulating cardiac movement and flow for further research.

2.2.2 Project plan general development

- Simulate $T2$ relaxation time decay in vitro:
  - Preparation of paramagnetic solution.
  - Theoretical calculation of solution $T2$.
  - $T2$ measurement by BOLD sequence.
  - $T2$ measurement by SE sequence.
  - Result comparison and analysis.
- Develop parametric model to fit $T2$ values dependent on hole blood oxygen saturation:
  - Blood extraction and deoxygenation.
  - $T2$ measurement by BOLD sequence with in-vitro samples.
  - Establish relationship between oxygen level and $T2$ values for each sample.
  - Identification of model and calculation of correlation parameters.
- Apply previously calculated parameters in-vitro to estimate the oxygen saturation in-vivo:
  - In-vivo heart BOLD measurement.
  - Estimation of saturation oxygen values.
- Identify factors affecting accuracy and precision of data estimates:
  - Heart phantom analysis of flow affecting measurement.
  - Compare results with previous documentation.
  - Determine necessary corrections in sequence.
  - Recognize limitations and improvements of study method.

2.3 Biological background

2.3.1 Fetal Circulation

Fetal lungs are not functional during the gestational period, therefore the only source of oxygen comes from the umbilical cord. This vital conduct consists of one umbilical vein and two umbilical arteries. The umbilical vein provides the fetus with rich oxygen blood with a saturation between 80% to 90%, where as the umbilical arteries carry all the deoxygenated blood out of the fetus. [29]

In Figure 2.1 is presented an anatomy model of the fetal heart. There are two main anatomic differences in comparison with a mature heart: the ductus arteriosus (connects the pulmonary artery with the aorta) and the foramen ovale (connects the right and left atrium).

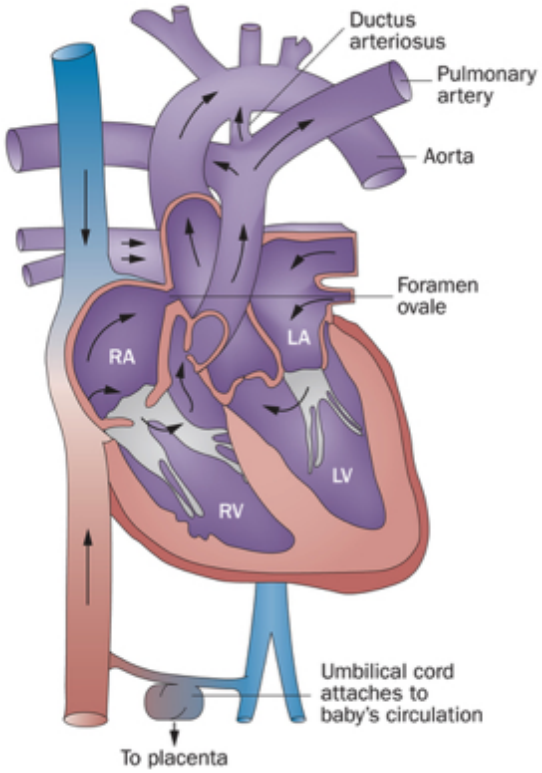

Figure 2.1: Fetal heart anatomy [29]

The fetal heart pumps with the only objective of delivering oxygen to the tissues. Fetal circulation process and their average oxygen levels are illustrated in Figures 2.2 and 2.3. [29]

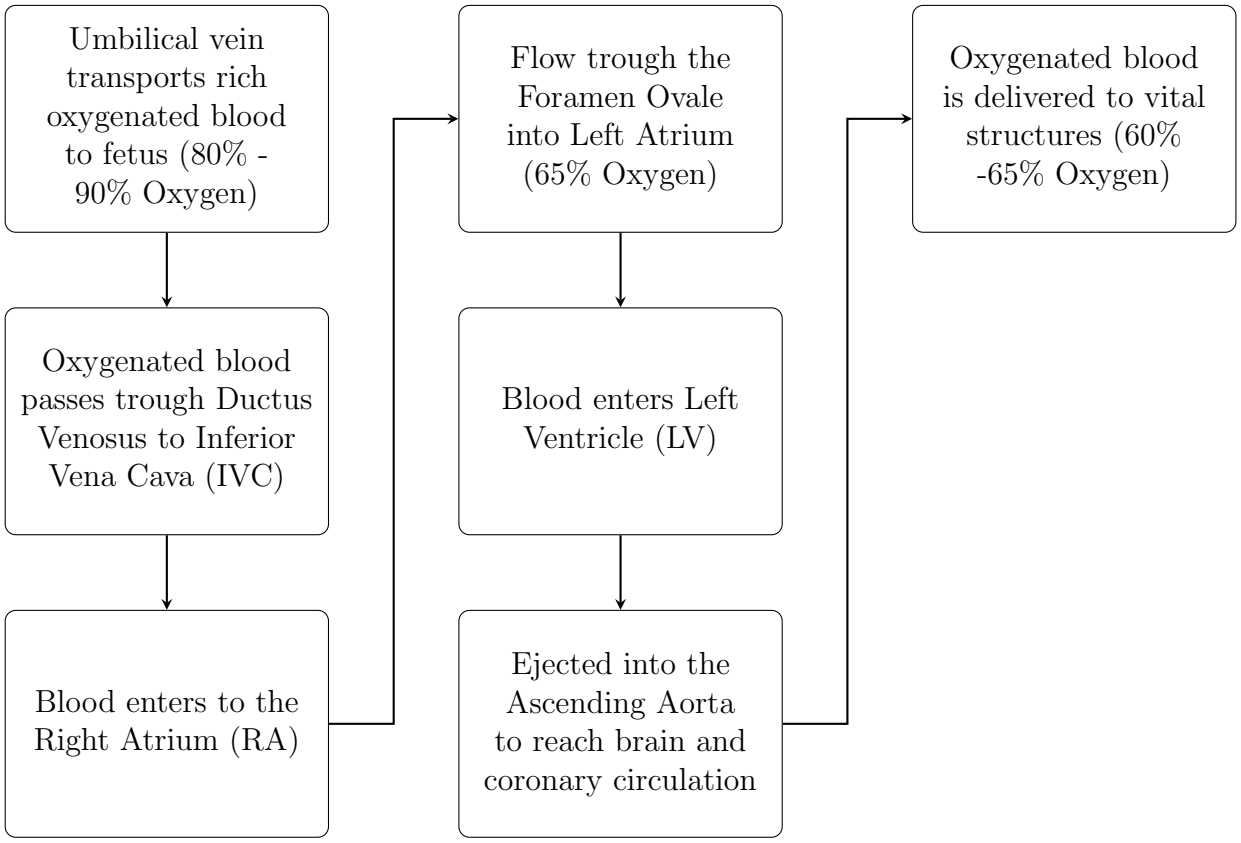

Figure 2.2: Oxygenated fetal blood path

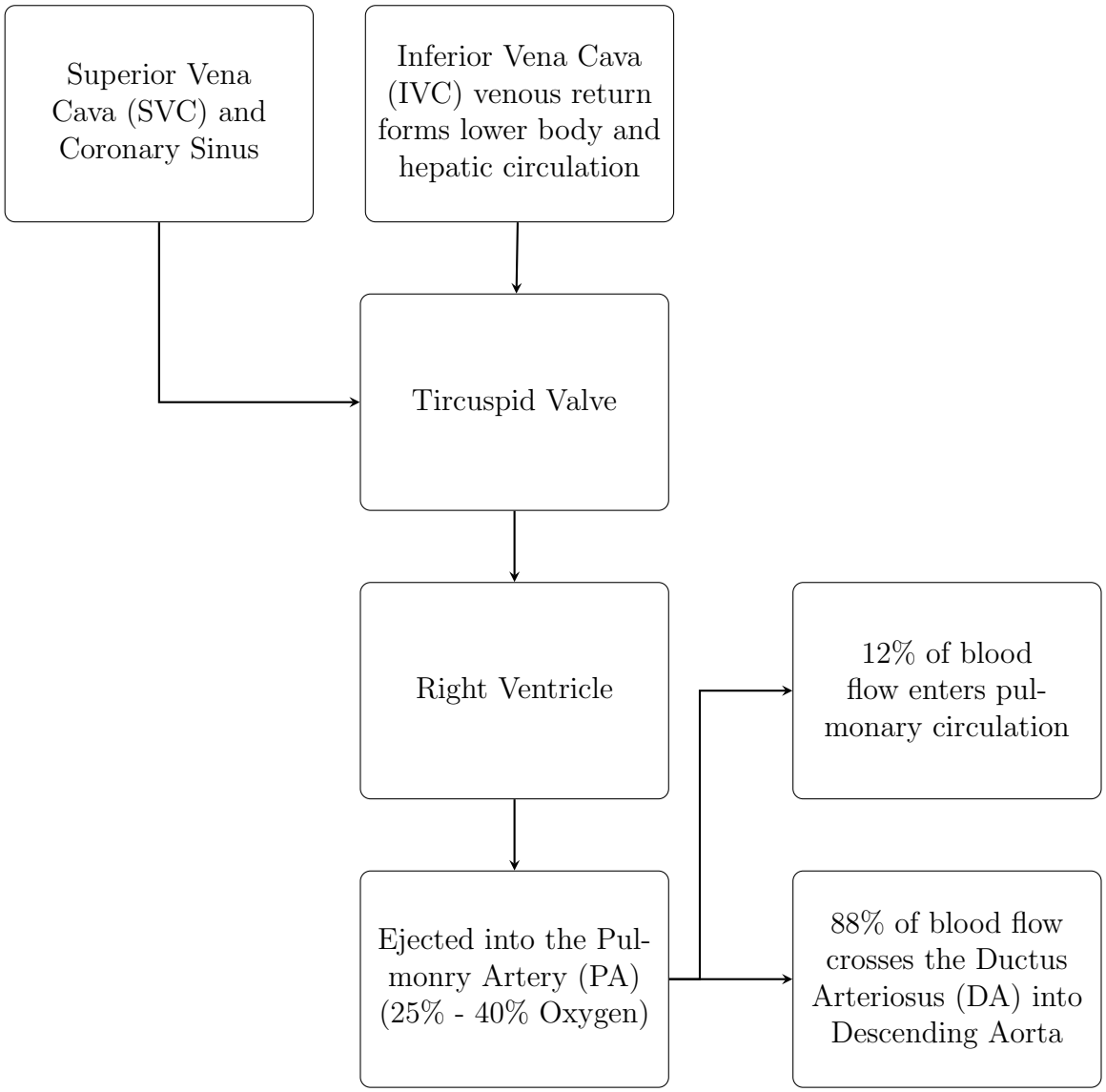

Figure 2.3: Deoxygenated fetal blood path

2.3.2 Hemoglobin Structure

Hemoglobin (Hb) is the protein contained inside red blood cells which transports oxygen to every tissue. This oxygen is to be used in the oxidative metabolism for the creation of cellular energy [42]. The hemoglobin molecule is a tetramer composed of four subunits (2-α and 2-β), each one of this subunits strongly binds a non-protein group named **heme**. See figure 2.4.

The heme group contains an iron atom which is responsible for binding the oxygen, this may be either in Fe_{2+} or Fe_{3+} state. If the heme group contains no oxygen, the molecule is named **deoxyhemoglobin**. In this case, the iron ion will be Fe_{2+} and it would have four impaired electrons per heme group. Meanwhile, if the heme group binds an oxygen molecule, the iron ion oxidizes forming Fe_{3+} and it would contain no unpaired electrons, this molecule is called **oxyhemoglobin**. [42].

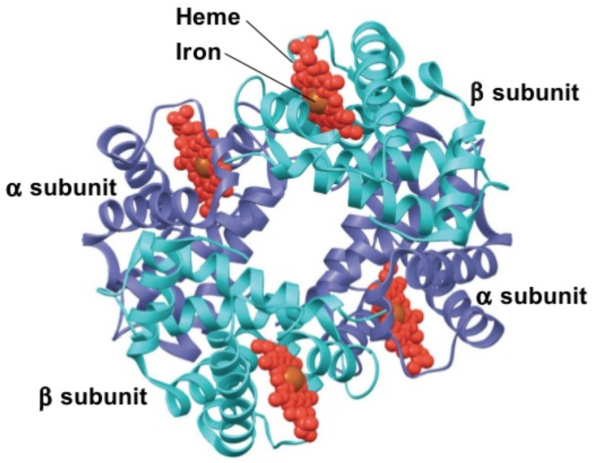

Figure 2.4: Subunits structure of hemoglobin. [42]

2.3.3 Magnetic susceptibility of hemoglobin

Schenck et al. defines **magnetic susceptibility** (X) as "a dimensionless constant that indicates the degree of magnetization of a material in response to an applied magnetic field" [39].

In other words, when matter interacts with an external magnetic field (B_0), a polarization (J) inside the matter is created. If the internal polarization opposes the external field, the magnetic lines are dispersed and the local field is reduced, this effect is known as **diamagnetism**. However, if the internal polarization is in the same direction as the external field, the magnetic lines are gathered within the object and the local magnetic field increases, resulting in **paramagnetism**. See Figure 2.5

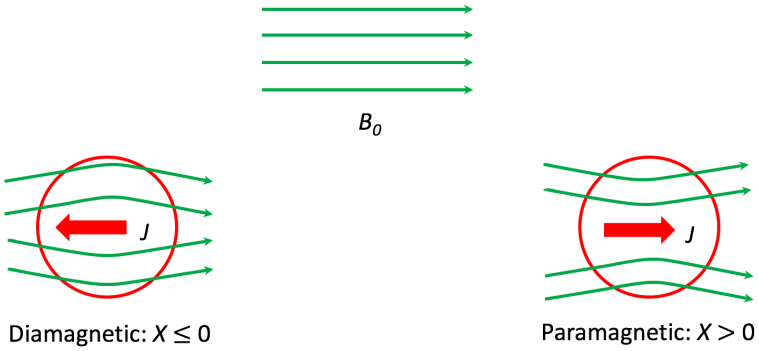

Figure 2.5: Magnetic susceptibility of diamagnetic and paramagnetic elements. Where B_0= external magnetic field, J= internal polarization and X= magnetic susceptibility coefficient.

The matter's magnetic susceptibility depends on the number of unpaired electrons in the molecules, by the following proportion [39]:

$$X \propto N(N+2) \tag{2.1}$$

$$R2 \propto X^2 \tag{2.2}$$

Where:
X= Magnetic susceptibility coefficient
N= Number of unpaired electrons
$R2$= $\frac{1}{T2}$= Relaxation rate (ms^{-1})
$T2$= Relaxation time (ms)

Based on equation 2.1, a material is considered diamagnetic when $X \leq 0$, and paramagnetic when $X > 0$. In the case of an hemoglobin molecule, the number of unpaired electrons in the heme group defines its magnetic susceptibility. Based on that principle, deoxyhemoglobin contains 4 unpaired electrons per heme group ($X \propto 96$) therefore is considered paramagnetic, whereas oxyhemoglobin contains 0 unpaired electrons ($X \propto 0$) is diamagnetic [32].

2.4 MRI physics overview

2.4.1 Spin properties

In quantum physics, the **spin** (s) is an atomic natural property like the electrical charge or mass. Protons, electrons, and neutrons possess a spin with either a value of $\frac{1}{2}$ (spinning clock-wise) or -$\frac{1}{2}$ (spinning counter-wise). [21, 35].

Knowing that all rotating particles produce magnetic fields, the spin property gives the particles a **magnetic moment vector** (μ) which direction indicates the rotating axis, and magnitude the amount of magnetism generated by the particle. [21,35]. See Figure 2.6

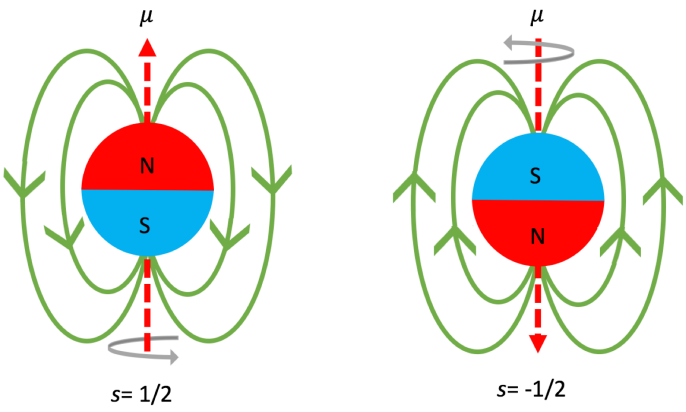

Figure 2.6: Spin representation with magnetic field lines (green), and magnetic moment vector (μ) (red). Where s is the atomic spin value

When a proton is subjected to an external magnetic field (B_0), the magnetic moment (μ) aligns itself with the external field. In this case, the particle can adopt two configurations: low energy state (N^-) or high energy state (N^+). The protons with N^+ will line up against the magnetic field B_0 [16]. See Figure 2.7

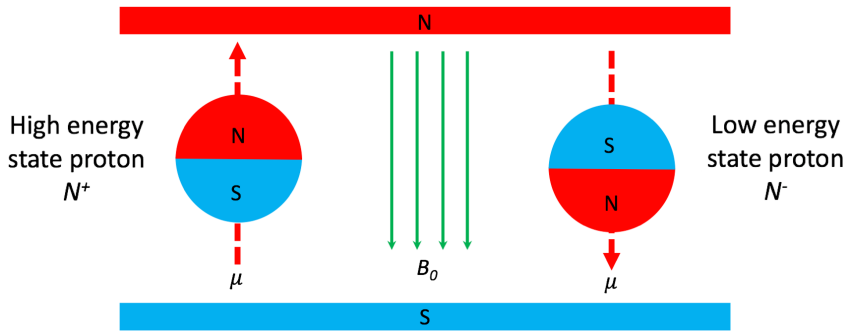

Figure 2.7: Energy states configuration for protons in an external field B_0

2.4.2 Precession

All protons rotate (or precess) at certain frequency called **Larmor frequency** (f), that is proportional to the magnetic field and the gyromagnetic ratio of the molecule. See Equation 2.3, [14, 21, 35].

$$f = \gamma B_0 \tag{2.3}$$

Where:
f = Precession frequency in MHz
γ = Gyromagnetic radio in MHz/Tesla
B_0= External magnetic field in Tesla

For a photon to cause a transition between the two energy levels of the spin (N^- to N^+), it should have the same frequency as the precession. In the case of a 3 Tesla MRI magnetic field, the Larmor frequency of a hydrogen atom is 127.74 MHz, that means that a photon of 127.74 MHz is necessary to cause a transition from N^- to N^+. [7, 35]

2.4.3 Net magnetization vector

The sum of all proton's magnetic moment vectors (μ) is called **net magnetization vector** (M), and its magnitude is proportional to the amount of high and low energy protons ($N^- - N^+$) under the same external field B_0. See Figure 2.8.

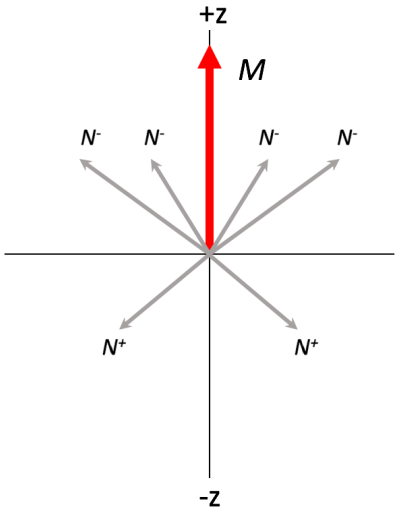

Figure 2.8: Representation of net magnetization vector (M) in red, and proton magnetic moments (μ) in gray. Following convention, N^+ are placed in -z axis because they orientate against the magnetic field.

2.4.4 T1: spin-lattice relaxation time and longitudinal magnetization

Longitudinal magnetization (M_z) is the component on z axis of the net magnetization vector M. Before the radio-frequency pulse is applied, M points to the same direction as the external magnetic field B_0 which by convention is aligned to the +z axis. [7, 14, 37]. See Figure 2.9a

When the radio-frequency wave is applied to the nuclear spin system, N^- absorb that energy and change their orientation to a N^+ state. Meanwhile, the longitudinal magnetization M_z decreases and approaches to zero [21, 37]. See Figure 2.9b

When all protons reach the N^+ state, the longitudinal magnetization M_z is considered to be negative [21, 37]. See Figure 2.9c

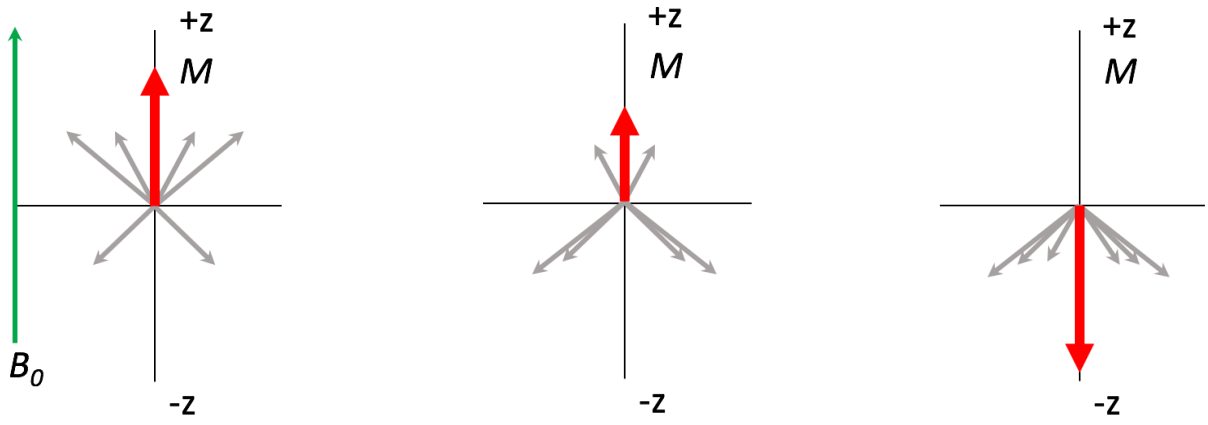

(a) (b) (c)

Figure 2.9: (a) M at equilibrium before the pulse, (b) When energy is applied, protons change to a high energy state and are aligned against the magnetic field, (c) All protons in a high energy state resulting in a negative M vector.

After applying the radio-frequency pulse, the system will return gradually to its initial state. The time constant that measures how M_z returns to its equilibrium value is called **spin-lattice relaxation** or $T1$, and it is described by the following equation: [21, 37]

$$M_z = M_0(1 - 2e^{-t/T1}) \tag{2.4}$$

Where:
M_z= Longitudinal magnetization
M_0= Equilibrium magnetization
t= Time after displacement of M_z
$T1$= Spin-lattice relaxation time

2.4.5 T2: spin- spin relaxation time and transversal magnetization

When the radio-frequency pulse is applied to the protons, they start precessing at the same frequency entering to a temporary phase coherence into the xy plane, this pulse is also known as 90° pulse since M is turned by 90°. In this state, the transversal magnetization vector (M_{xy}) reaches its maximum level. [7, 14, 37]

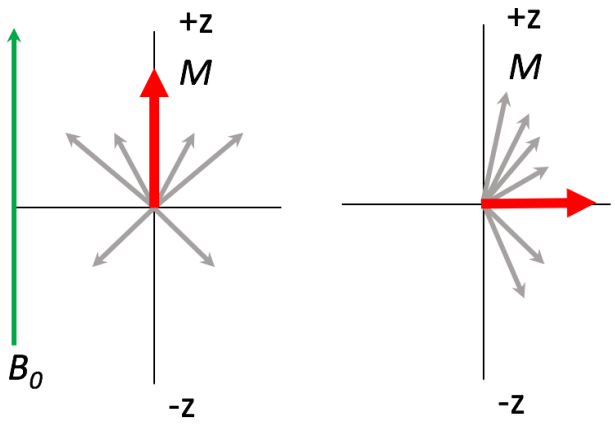

(a) (b)

Figure 2.10: (a) M at equilibrium before the pulse, (b) M grows on the xy after RF pulse is applied

After the radio frequency signal has stopped, each spin starts dephasing and the previously absorbed energy is dissipated to the surrounding tissues as heat causing M_{xy} to decay. [21].

The **spin-spin relaxation time** or $T2$, is the decay time of M_{xy} until it reaches equilibrium once again [21, 37], and it is described by equation 2.5:

$$M_{xy} = M_0 e^{-t/T2} \tag{2.5}$$

Where:
M_{xy}= Transverse magnetization
M_0= Equilibrium magnetization
t= Time after displacement of M_{xy}
$T2$= Spin-spin relaxation time

In addition, transverse magnetization is affected by inhomogeneities across the external magnetic field B_0 known as $T2inhomo$. In practice, the combination of pure $T2$ caused by proton interaction and the inhomogeneities of B_0 is what results in the decay of M_{xy}. This combined time variable is known as $T2^*$ and it is determined by Equation 2.6:

$$T2^* = T2 + T2inhomo \tag{2.6}$$

Where:
$T2^*$= Total transverse magnetization
$T2$= Relaxation time affected by proton interaction
$T2inhomo$= Relaxation time affected by field inhomogeneities in B_0

At the end of the excitation pulse, M_{xy} generates a current that is detected by the MRI coil, subsequently forming an image [47].

It is worth to mention that this M_{xy} signal is not constant, instead it is decaying at a rate described by equation 2.5 and this decay phenomena its named "free induction decay "or "FID". [19]

2.4.6 T1 and T2 processes

Until now, longitudinal (M_z) and transversal (M_{xy}) magnetization were described separately. However these two processes occur simultaneously as summarized below: [2, 4, 7, 14, 16, 19, 35]

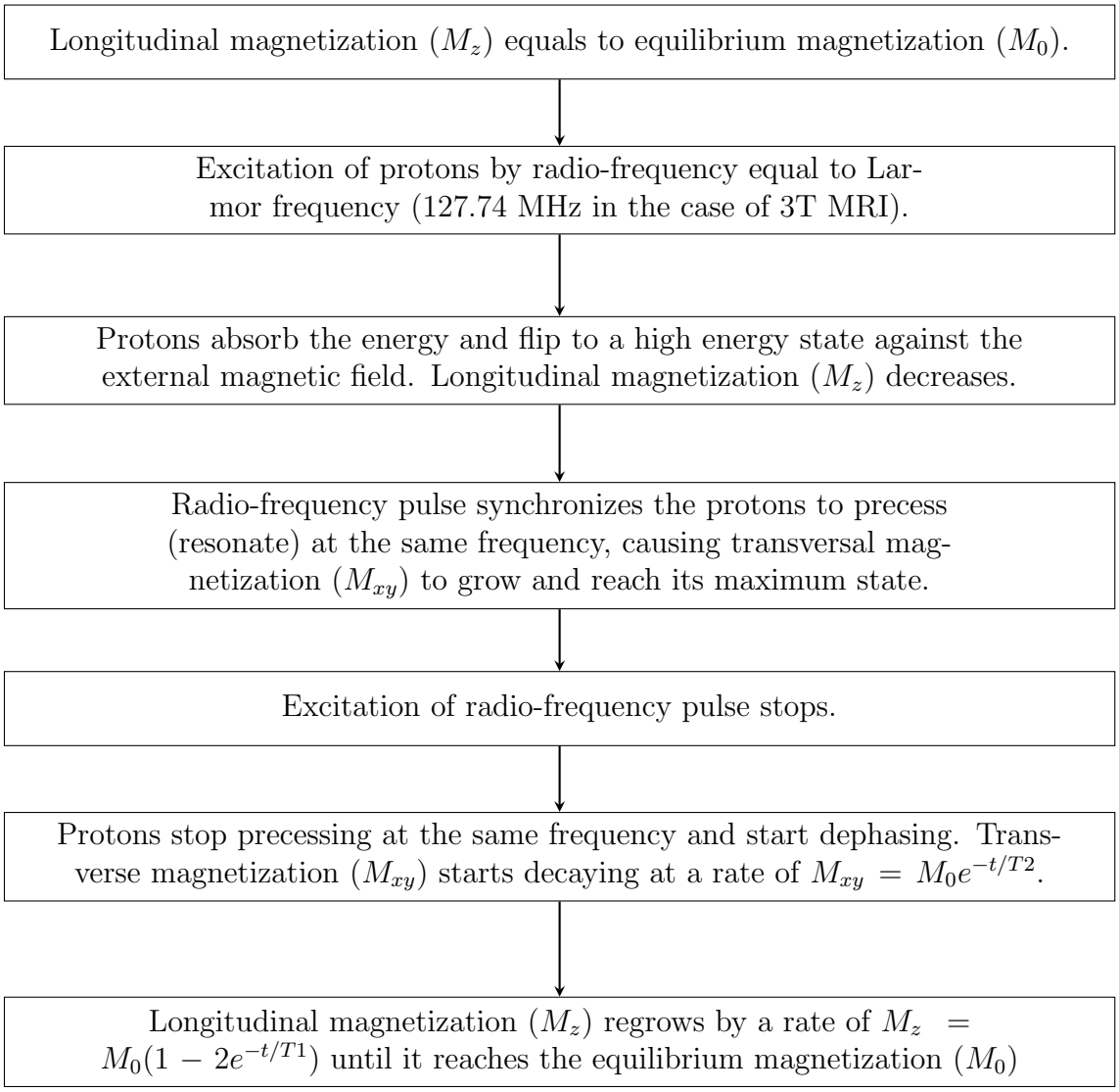

Figure 2.11: Summary of longitudinal (M_z) and transverse magnetization (M_{xy}) processes

2.5 MR pulse sequences

As mentioned above, MRI scanners only detect photon signals if these have transverse magnetization (M_{xy}), hence a radio-frequency pulse is needed to produce these.

The radio-frequency pulses produced by the MRI are named **pulse sequences** and are used to generate photon's longitudinal and transverse magnetization. The fundamental sequences are mentioned in Table 1. [2]

Type of MR Signal	**Type of pulse**
Free induction decay (FID)	90° pulse (from+z axis to +y axis)
Spin echo (SE)	90° + 180° pulse (from +y axis to -y axis)
Gradient echo (GRE)	90° pulse and gradient reversal

Table 1: Principal MRI pulse sequences

2.5.1 Free induction decay (FID)

After the radio frequency is turned off, protons release the absorbed energy. If nothing is affecting the magnetic field's homogeneity, all the protons will spin at the same resonance frequency. The signal unaffected by any gradient is known as Free Induction Decay or FID, nevertheless it does not offer positional information [14, 16, 21]. The details of this process where already explained in Section 2.4.5.

The initial amplitude of the signal is determined by the magnetization vector (M) that has been directed onto the xy-plane, which respectably depends on the flip angle α. The maximum signal is obtained when the flip angle is 90° (sin(0°)=0, sin(90°)=1). See Equation 2.7

$$S = M_0 sin(\alpha) e^{-t/T2^*} \tag{2.7}$$

Where:
S= Signal
t= Time after displacement of M_{xy}
M_0= Equilibrium magnetization
$T2^*$= Total transverse magnetization

One single radio-frequency pulse and its FID illustrated in Figure 2.12.

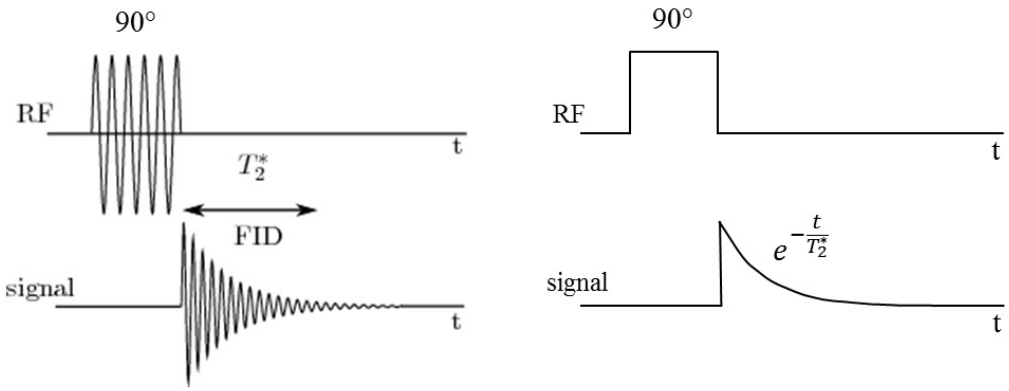

Figure 2.12: Free induction decay. The obtained signal decay curve is actually the signal envelope (right), the actual signal oscillates at the resonance frequency in MHz (left). [21]

2.5.2 Spin echo (SE)

In order to only detect $T2$ and eliminate the consequences of local magnetic field inhomogeneities, a 180° rotation of the protons is necessary. They will continue precessing, nevertheless they will refocus along the -y axis. [2, 14]. A diagram of three spin echo repetitions is shown in Figure 2.13

Spin echo sequences occur in three main steps: [2, 7, 19]

1) 90° pulse: translates the net magnetization vector from +z to +y.

2) 180° pulse: refocuses the precession of protons and reverse the effects of local magnetic field homogeneities. The net magnetization vector translates from +y to -y, the refocusing of protons in the -y axis is called **echo** and the time it occurs is known as **echo time** (TE).

3) **Repetition time** (TR) is the time between each repetition of the sequence. This time is needed to allow the longitudinal magnetization to recover.

In addition to the RF pulses, the spatial location gradients are also used to acquire a better signal: [2]

1) **Slice gradient** determines which protons get excited and therefore they turn on during any excitation RF pulse (90°or 180°).

2) **Phase gradient** is turned on to generate the phase shifts.

3) **Read-out** is when the MRI scanner acquires the signal.

3) **Frequency gradient** is turned on at the same time as the read-out since they alter the precession frequency.

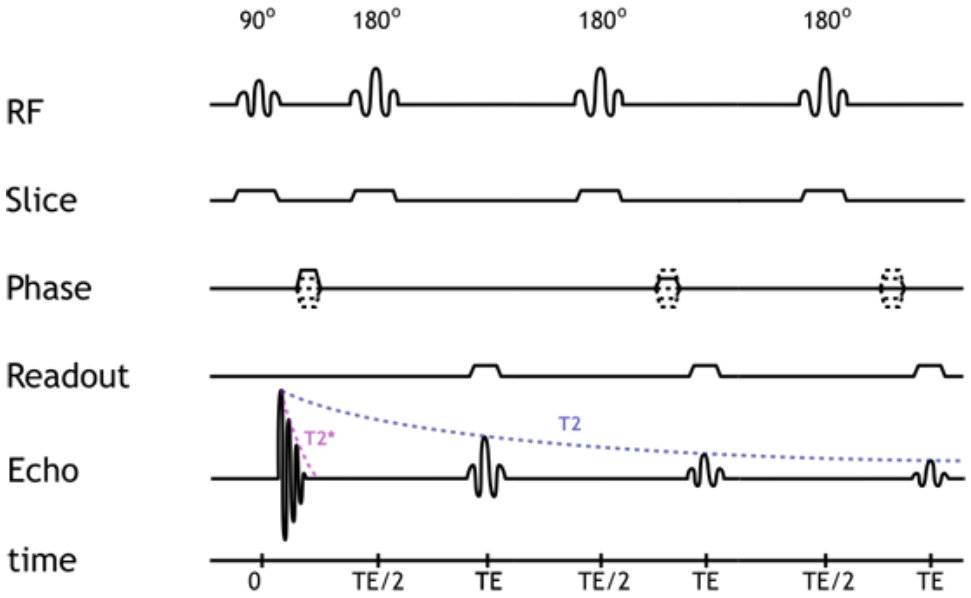

Figure 2.13: Spin echo diagram [2] Frequency gradient is not pictured since is activated at the same time as read-out.

Rapidly and regularly applying 180° pulses reduces the range of frequencies a spin experiences before it is refocused. This train of pulses restores the coherence of spins dephased due to $B0$ inhomogeneities, causing that the SE measured signal depends only on $T2$ [2, 19, 36].

2.5.3 Gradient- recalled echo (GRE) and Steady-State Free Precession (SSFP)

GRE sequences are more sensitive to field inhomogeneities, therefore its signal is based on $T2^*$. Unlike SE sequences, GRE creates an echo by reversing the frequency encoding gradient instead of using a 180° RF pulse. This gradient reversal, causes the formation of an echo within one FID. [21, 51].

A diagram of a gradient echo sequence is shown in Figure 2.14.

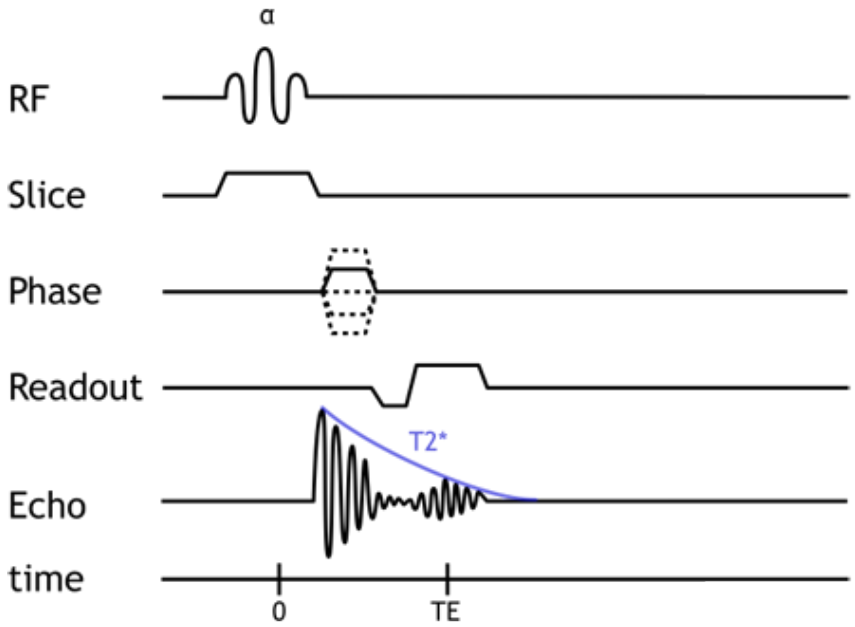

Figure 2.14: Gradient echo diagram. [2]

Gradient echo sequences are formed by three main steps: [2, 19, 51]

1) α pulse: less than 90° RF pulses are applied to always maintain longitudinal magnetization.

2) Activation of gradient: causes a calibrated change in local magnetic fields, altering the resonance frequencies of the protons in a specific area. The gradient causes an accelerated dephasing of protons.

3) Gradient reversal: applied with opposite polarity but same strength resulting in rephasing of protons and forming an echo.

Repetition times in GRE sequences are much faster as the excitation pulse applied is less than 90°, which promotes a rapid recovery of the longitudinal magnetization. [2, 51]

A **Steady-State Free Precession (SSFP)** is a special type of GRE sequence that refocus the residual M_z and M_{xy} in each repetition until it reaches equilibrium or "steady state" [11].

This steady-state is created by keeping the TR shorter than the $T2$ relaxation time of the tissue, hence the M_{xy} does not decay completely before the next repetition pulse is applied. This residual M_{xy} will be added into the M_z in the next excitation; producing an equilibrium between the two magnetizations after several pulses. [11, 51]

Many SSFP sequences tend to balance their gradients, meaning that for every positive gradient another opposite is added with the same magnitude. As a result, the net gradient-induced dephasing over a TR interval is zero [11]. This gradient balancing is shown in Figure 2.15.

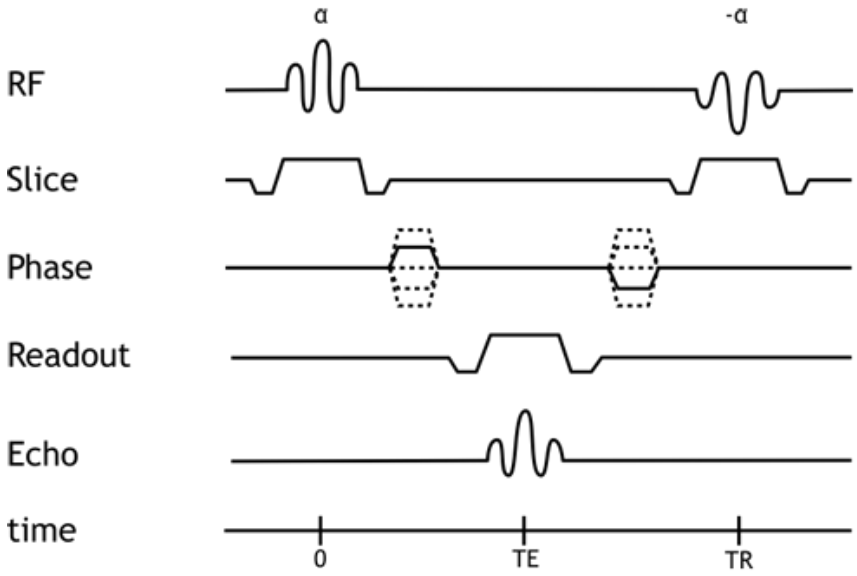

Figure 2.15: Steady- State Free Precession diagram. [11]

Additionally a SSFP produces two types of signals: A FID after excitation with the immediate RF pulse, and a spin echo (SE) formed when the residual echo from the previous pulse is refocused by the following echo. [11].

Because of their balanced echo rephasing, these type of sequences present low sensibility to motion and flow [11, 51], therefore they will be applied in this study as mentioned in Section 3.1.

2.6 BOLD

Blood oxygenation level dependent (BOLD) imaging was first described by Seiji Ogawa in 1990. He discovered that the imaging contrast could be changed depending on the blood oxygen level, using a gradient-echo pulse in a 7 Tesla magnetic field. [31].

The revolutionary work of Ogawa promoted great interest in the medical fields for BOLD techniques. Initial studies presented MR detectable changes in cerebral blood flow and oxygen metabolism during stimulation [8]. From that moment forward, this technique has been used to analyze the relationship between blood flow and neuronal activity [6, 23, 48], and in recent years in cardiology studies to calculate oxygen levels and abnormal cardiac function [10, 15, 27, 28, 40, 49].

In principle, BOLD sequences depend upon the relaxation values of blood in MRI, and could be used in the future as an alternative for monitoring blood oxygen levels non-invasively.

Paramagnetic substances, such as deoxyhemoglobin, have a high magnetic susceptibility coefficient, therefore their magnetization is greater than diamagnetic substances (i.e oxy-hemoglobin) when placed in an external magnetic field. This effect creates local regions of magnetic inhomogeneity (see Section 2.3.3), which consequently leads to rapid dephasing of spins and rapid $T2^*$ signal loss on GRE images. [4, 17].

Additionally, this local regions with different magnetic susceptibilities produce small magnetic gradients that facilitate the diffusion of water protons across the erythrocyte membranes. This creates a local field gradient around the cells and enhances the loss of phase coherence, which in turn decreases $T2$ signal intensity in SE images. [17, 46, 50]

In Figure 2.16 the dependency of $T2$ on magnetic susceptibility is shown. Oxyhemoglobin has a low internal magnetization (red arrow) due to its small magnetic susceptibility coefficient which results in an homogeneous local field gradient and low water proton diffusion across erythrocyte membranes, and therefore a slow $T2$ relaxation. On the other hand, deoxyhemoglobin has a high intern magnetization (red arrow) that causes a higher local field gradient and increased proton diffusion, resulting in additional spin dephasing and faster $T2$ relaxation. [4, 32, 42, 50]

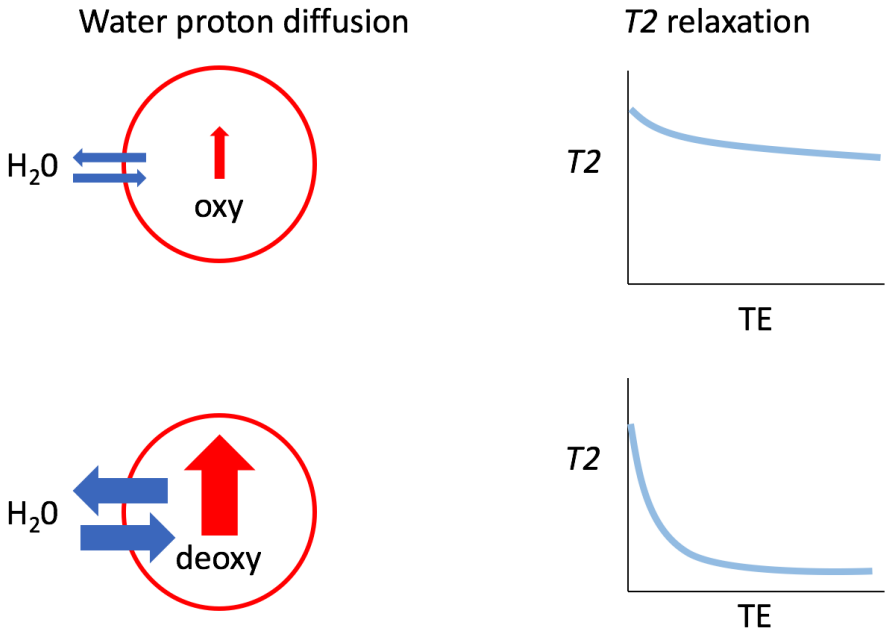

Figure 2.16: Water proton diffusion for deoxy- and oxy- hemoglobin cells and the effect that their intern magnetization (red arrow) has over the $T2$ relaxation times on an MRI scan.

3 Method

3.1 Sequences

To create a BOLD sequence an initial $T2$ preparation pulse followed by a balanced- SSFP sequence were used.

As previously stated in Section 2.5.3, GRE sequences depend on $T2^*$. Nevertheless, when the echo is recorded close to the middle of the interval ($TE \approx \frac{T2}{2}$), balanced sequences present a dependence on $T2$ [2,38]. This allows the measurements and data processing to be based on $T2$ values.

The BOLD sequence for all tests had the following parameters: slice thickness= 4 mm, TR= 3.7 ms, TE= 1.8 ms, Phase encoding steps= 87, Matrix size= 88x87, flip angle= 35°, total acquisition time= 61 s. This sequence was developed by Philips GmbH in collaboration with Dr. rer. nat. Hendrik Kooijman, Senior Clinical Scientist.

In Section 3.2 a Spin Echo (SE) sequence was used to compare $T2$ values obtained by calculations and BOLD sequence. (slice thickness= 4 mm, TR=1024 ms, TE=20 ms, Phase encoding steps= 87, Matrix size= 88x87, flip angle= 90°, total acquisition time= 986 s).

Measurements of phantom's flow, volume and velocity in Section 3.7 were made using a GRE Cine Sequence (18 slices, 30 phases, TR= 6.5 ms, TE= 3.4 ms),where as the wall motion was evaluated with a GRE sequence (TR= 2.9 ms, TE= 1.5 ms).

3.2 Simulation of different $T2$ values with aqueous paramagnetic phantom

The below mentioned experiment has as objective to measure $T2$ relaxation values performing a SE and BOLD sequence in a steady solution. Additionally a further comparison between the calculated theoretical results and the ones obtained in the experiment is performed. The results are described in Section 4.1.

3.2.1 Sample preparation

Contrast agents are frequently used to simulate desired relaxation values and mimic the relaxivity form anatomical tissues. The relaxation time in presence of a contrast agent is determined by [27]:

$$R2 = \frac{1}{T2} = (\frac{1}{T2dia}) + r_2C \tag{3.1}$$

Where:

$R2$= Solution relaxation rate (ms^{-1})
$T2$= Solution relaxation time (ms)
$T2dia$= Solvent relaxation time (ms)
r_2= Transverse relaxivity of the contrast agent ($mM^{-1}s^{-1}$)
C= Concentration of contrast agent (mM)

Manganese (II) chloride ($MnCl_2$) was selected as contrast agent and dissolved with distilled water in different concentrations. The probes were prepared in 7.5 ml containers.

The following concentrations of $MnCl_2$ were used for this test:

Sample Nr.	1	2	3	4	5	6
$MnCl_2$ (mM)	0	0.04	0.05	0.08	0.1	0.2

Table 2: Sample $MnCl_2$ concentrations

To calculate $T2$ for each concentration a value of $r_2 = 117\ mM^{-1}s^{-1}$ was considered [44] in Equation 3.1. Subsequently the containers were placed inside a water bath and scanned in a 3T MRI (Philips Ingenia, The Netherlands).

To obtain the signal intensity of each prove, a ROI (Region of Interest) with area of 98.20 mm^2 was drawn in the resulting images. Thereafter, $T2$ values were calculated from the average signal using monoexponential fitting of the following function [25]:

$$S = S_0 e^{-TER2} \tag{3.2}$$

Where:
S = Probe signal at a particular TE (a.u.)
TE = Echo time (ms)
S_0= Equilibrium signal from the MRI (a.u.)
$R2$= Relaxation rate (ms^{-1})

S_0 and $R2$ were the parameters estimated in this fitting. The results for the $T2$ and $MnCl_2$ relationship obtained with the experiment were compared with the theoretical $T2$ from Equation 3.1.

3.3 Calibration study: Acquisition of coefficients in adult blood (in-vitro)

Since fetal blood follows a more complex acquisition process, it was decided to test the quantification of $T2$ values first from adult blood.

The below mentioned test has as objective to quantify and correlate different oxygen levels with $T2$ relaxation values of adult blood. The obtained results are the fitting coefficients that would help to predict the oxygen values in-vivo. An overview of the executed steps is provided in Figure 3.1 and results are presented in Section 4.2.

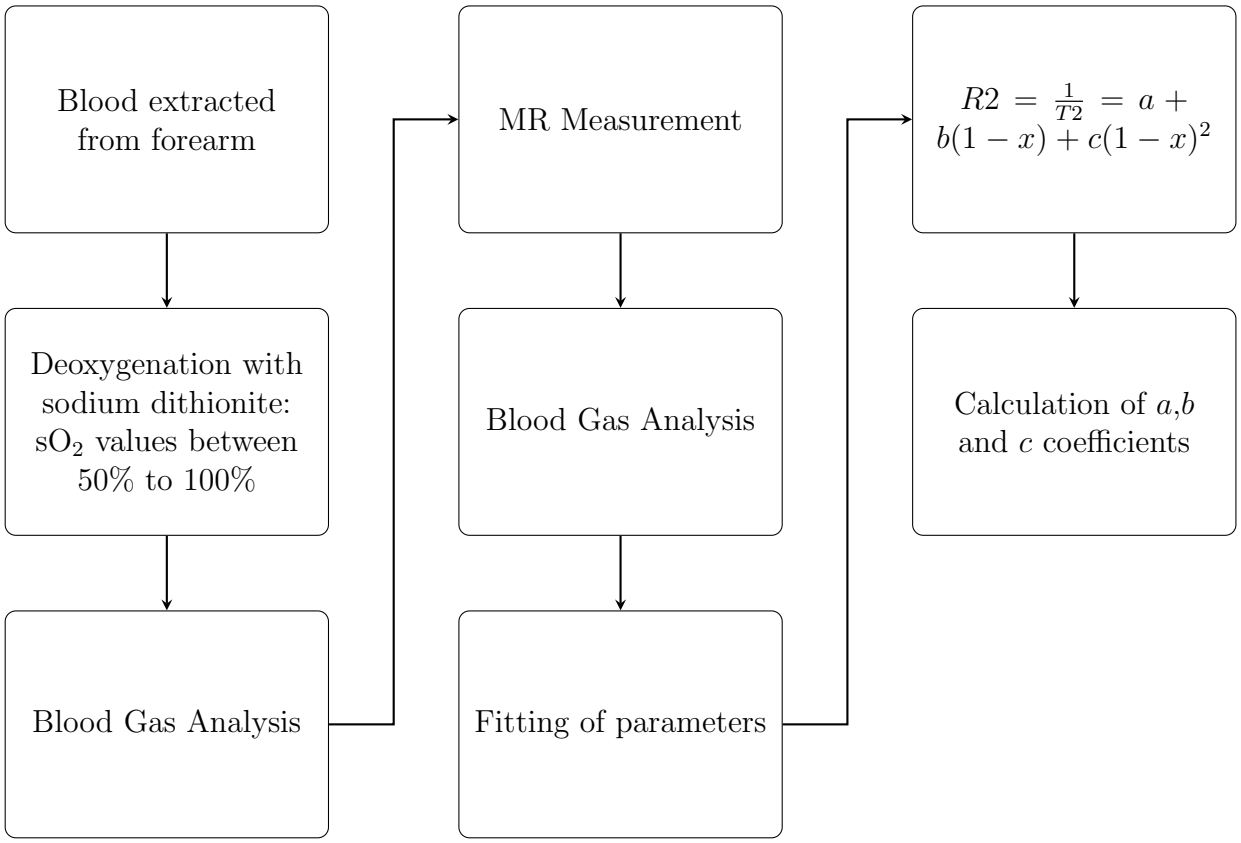

Figure 3.1: Flow chart for coefficients acquisition in adult blood test

For simplicity, all graphs represent $T2$ values from the fitting. Nevertheless all the calculations were made using the relaxation rate values ($R2 = \frac{1}{T2}$).

3.3.1 Sample recollection and deoxygenation

Whole blood samples were obtained by forearm venipuncture from three healthy human subjects (mean age= 29) and collected in containers S-Monovette 7.5 ml LH-Gel (Sarstedt, Germany).

To achieve 100% oxygen level, the containers from all samples were opened and exposed to normal air for an average time of 2 hours. Sodium Dithionite ($Na_2S_2O_4$) was added to one sample with a proportion of 2.5 mg per 1 ml of blood to achieve an sO_2 level of 0%. Afterwards, oxygenated blood was mixed with the 0% sample to acquire different oxygenation values.

3.3.2 Blood Gas Analysis

The oxygen levels of the samples were measured before and after the MR study by a blood gas analyzer ABL90 FLEX (Radiometer Medical, Denmark) to assure that the same oxygenation levels were maintained during the study. The oxygen values for every sample are presented in Section 4.2 Table 4. If the oxygen level changed during the scan, the average value was considered for the calculations.

3.3.3 MR measurement

The samples were mounted on a rotating plastic holder and submerged in water. The water temperature was maintained at 37°C through a set of plastic hoses connected to a water heater outside the MR examination room. The probes were turned between every sequence to avoid cell sedimentation. The complete experiment (from blood extraction to MRI scanning) was performed within a 6 hour period to assure integrity of the samples.

3.3.4 Calculation of fitting parameters

The images acquired were analyzed in DICOM Viewer 3.0 software (Philips, The Netherlands). A ROI (Region of Interest) with area of 98.20 mm^2 was drawn in every probe to determine the signal intensity.

$R2$ values were calculated using a monoexponential fitting of the average signal using Equation 3.2.

Based on [26, 33, 41, 53], the obtained $R2$ values were fitted by the following quadratic model to calculate the oxygen dependency:

$$R2 = \frac{1}{T2} = a + b(1 - x) + c(1 - x)^2 \tag{3.3}$$

Where:
$R2$= Relaxation rate (ms^{-1})
$T2$= Relaxation time (ms)
x= Oxygen saturation level (%)

In Equation 3.3 the coefficients a, b, c are dependent on the hematocrit level (Hct) by [26]:

$$a = a_1 + a_2 Hct + a_3 Hct^2 \tag{3.4}$$

$$b = b_1 Hct + b_2 Hct^2 \tag{3.5}$$

$$c = c_1 Hct(1 - Hct) \tag{3.6}$$

For this work the hematocrit level is considered to be constant with a mean value of Hct=0.44 throughout all the blood samples.

The fitting and estimation of S_0, $T2$ and x parameters, as well as a, b and c fitting coefficients were obtained by MATLAB programming. See Appendix A for code used to perform data fitting and calculation of fitting coefficients.

Afterwards, the model accuracy for every calibration fit was assessed by performing Pearson's chi-square test. See appendix B for MATLAB program developed to calculate the chi-square test value.

3.4 Validation study: Acquisition of oxygen values in adult blood (in-vivo)

The heart of a healthy adult was scanned using the designed BOLD sequence. As the oxygen values of these anatomical structures are well documented, these known parameters were used as a corroboration for the proposed model in Section 3.3. An overview of the executed steps is provided in Figure 3.2 and results are presented in Section 4.3.

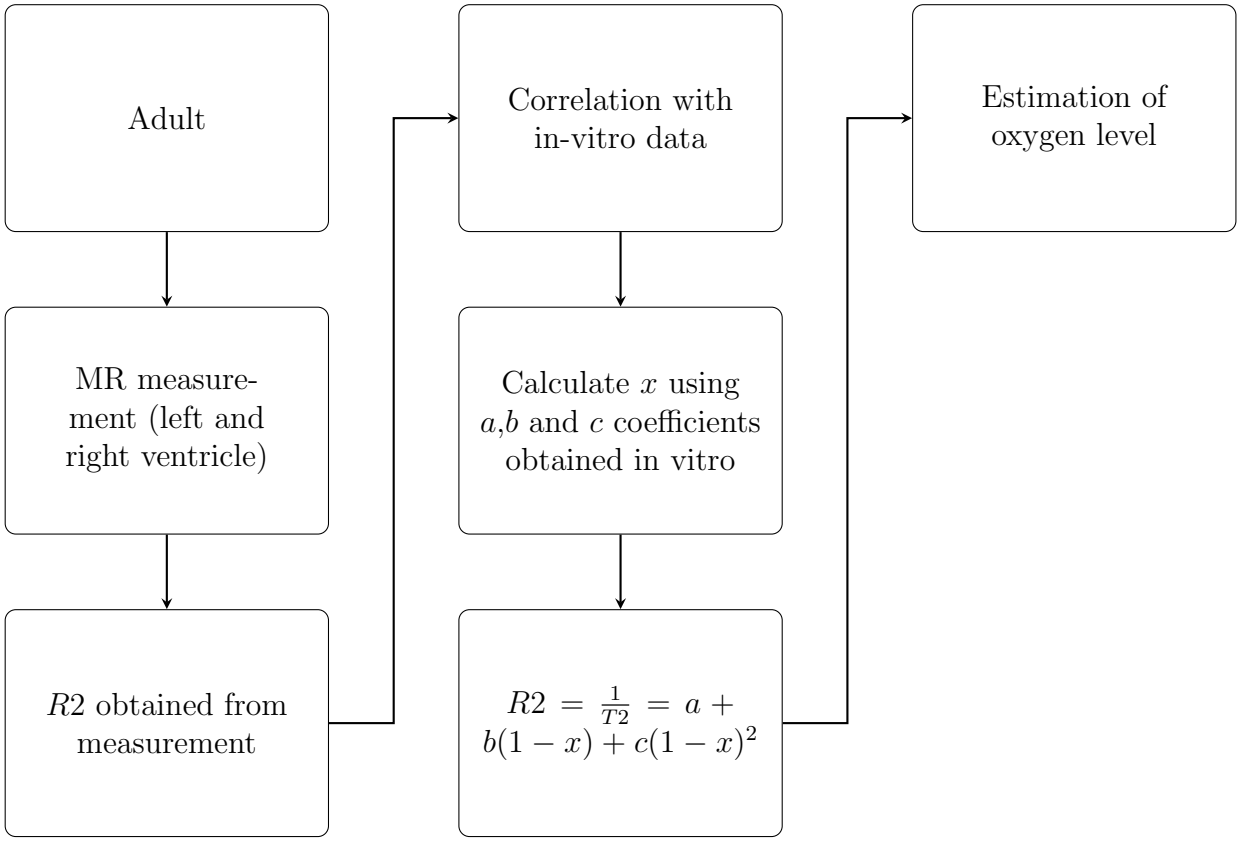

Figure 3.2: Flow chart of estimation of sO_2 in adult (in-vivo)

3.4.1 MR measurement

The subject was placed on top of the MRI table in a supine position and a radio-frequency body coil was placed in the chest area.The BOLD sequence was performed without triggering or breath - hold control.

3.4.2 Image Analysis: $R2$ values

The images acquired with the MRI were analyzed in DICOM Viewer 3.0 software (Philips, The Netherlands). A ROI (Region of Interest) with area of 98.20 mm^2 was drawn to determine the signal values from every sample.

$R2$ values were calculated using a monoexponential fitting of the average signal using the model previously mentioned in Equation 3.2.

3.4.3 Correlation with in-vitro data

The obtained $T2$ values and the fitting coefficients where used to estimate the oxygenation level using Equation 3.3. Afterwards, the $T2$ values obtained from the BOLD images where compared with the predicted $T2$ fitted values in-vitro.

3.5 Calibration study: Acquisition of coefficients in fetal blood (in-vitro)

The below mentioned test has as objective to correlate different oxygen levels with $T2$ relaxation values of fetal blood. The obtained results are the fitting coefficients that would help to predict the oxygen values in-vivo. An overview of the executed steps is provided in Figure 3.3 and results are presented in Section 4.4.

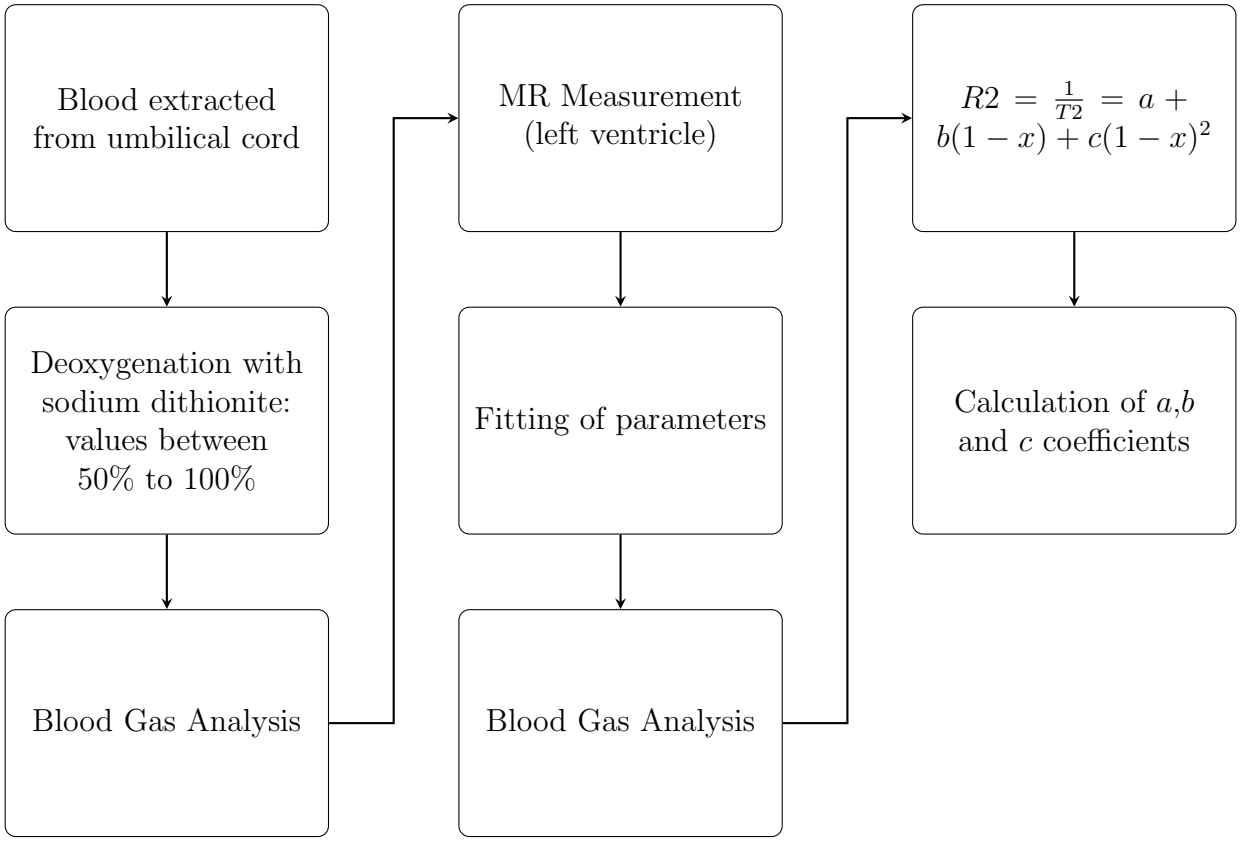

Figure 3.3: Flow chart for coefficients acquisition in fetal blood test

Sample recollection was performed by the UKE Hamburg Gynecology Department. Blood samples were extracted from the umbilical cord of two healthy newborns and collected in S-Monovette 7.5 ml LH-Gel containers (Sarstedt, Germany).

The deoxygenation process, blood gas analysis, MR measurements and calculation of fitting parameters were performed according to Section 3.3.

The remaining air inside the samples was removed inserting a syringe needle on top of the blood container and pushing the rod to eliminate the air. The oxygen values for every sample are presented in Section 4.4.

3.6 Validation study: Acquisition of oxygen values in fetal blood (in-vivo)

The heart of a 32 weeks fetus was scanned using the BOLD sequence. Same process as Section 3.4 was followed for image analysis and correlation of data. An overview of the executed steps is pictured on Figure 3.4 and results are presented in Section 4.5.

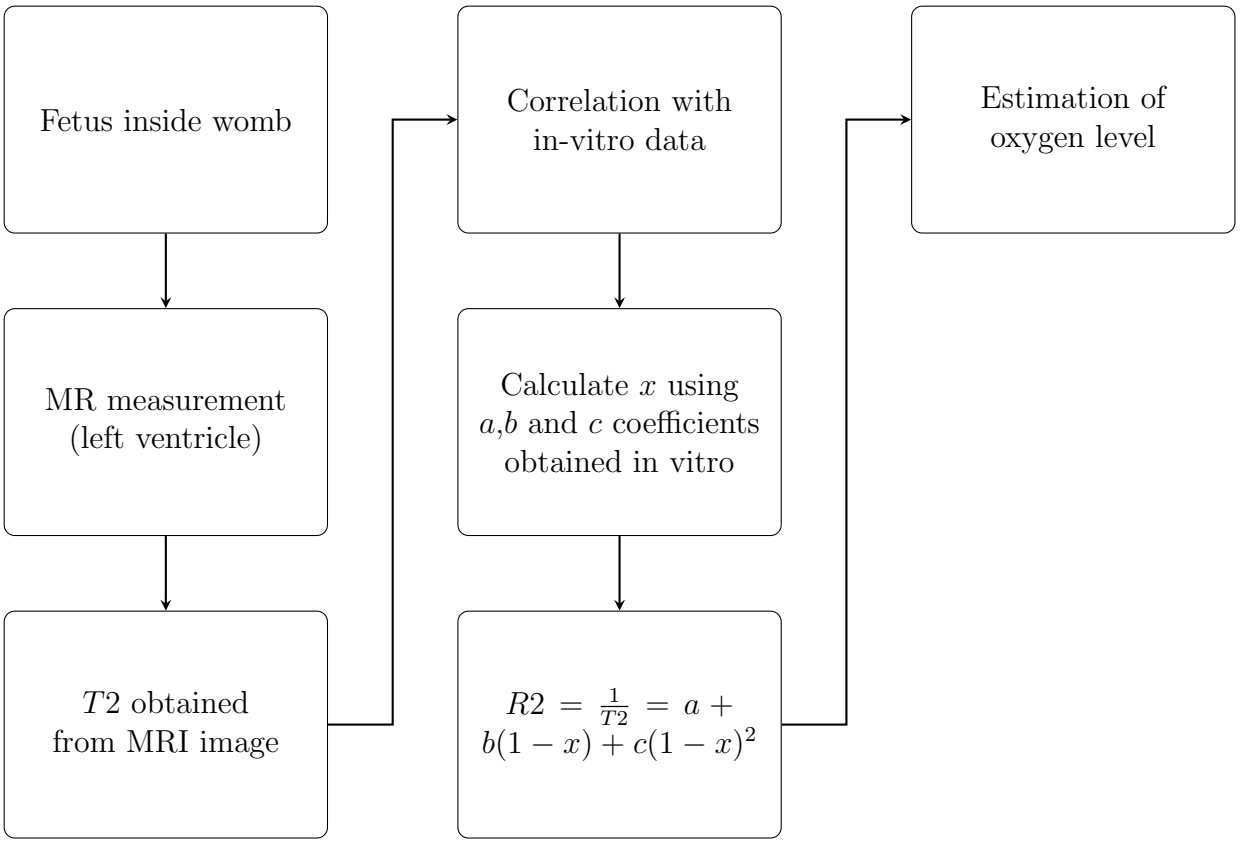

Figure 3.4: Flow chart of estimation of sO_2 in fetus (in-vivo)

3.6.1 MR measurement

Female pregnant patient was placed on the MRI table in lateral decubitus position and radio-frequency body coil placed in the abdomen area. The BOLD sequence was performed without cardiac triggering and non controlled breathing.

3.7 Simulation of cardiac volume, flow and velocity in fetal heart

The below mentioned test has as objective to simulate cardiac flow and velocity to further determine the effect of continuous and pulsatile flow in measurements performed with BOLD sequences.

3.7.1 Fetal heart phantom

An MRI compatible fetal heart phantom was produced to mimic dimensions, cardiac motion and internal blood circulation of a 37-weeks gestational age fetus. See Figure 3.5

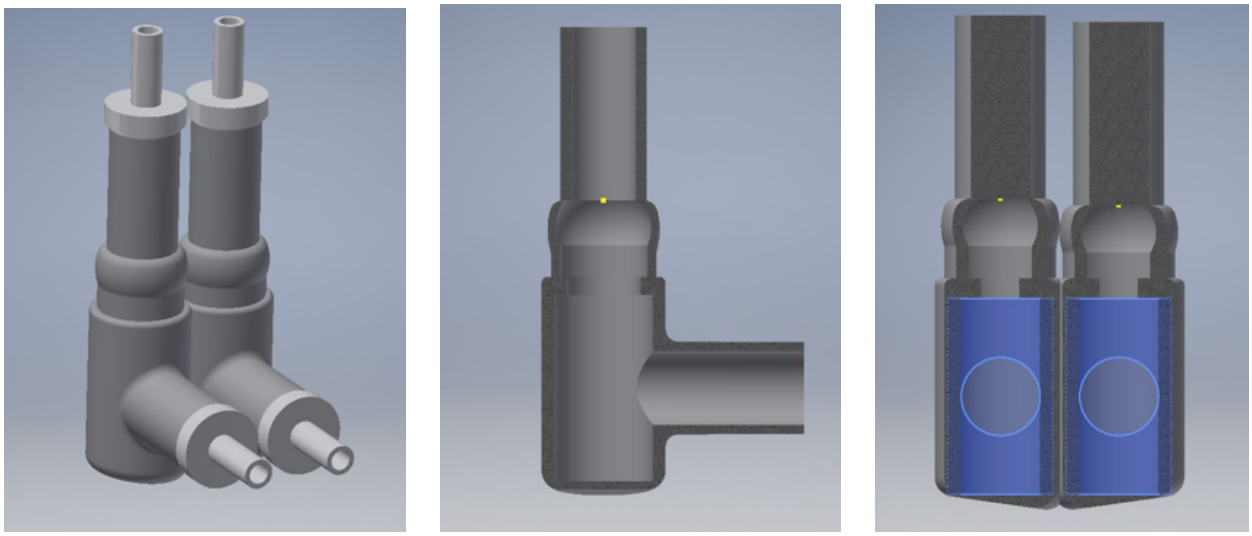

(a) (b) (c)

Figure 3.5: Physical model of heart phantom

The anatomical measures were based on literature [30] (right/left ventricular diameter= 215 mm, total height= 590 mm) to design a two-chamber structure polyamide mold (Solidworks, France). The mold was subsequently 3-D printed (Ultimaker, The Netherlands) and Room Temperature Vulcanization (RTV) silicone rubber (TFC Silikon,Germany) was poured inside the mold with a hardening time of 4 hours.

The heart was mounted inside a sealed water container and connected by 9 meters of hose to an hydraulic pumping system. The pulsatile flow was generated by an hydro-motor (Pentair/SHURflo, US) connected to two solenoid valves (NC 3/2 M&M International), these powered by a micro-controller (Arduino UNO AG, Italy) that simulates the cardiac heart cycle at frequencies from 1.25 to 4.5 Hz (75 - 270 bpm). See Annex D for Arduino code. The solenoid valves, as well as the hydro-motor were placed outside the MR unit due to their metallic constitution. See Figure 3.6

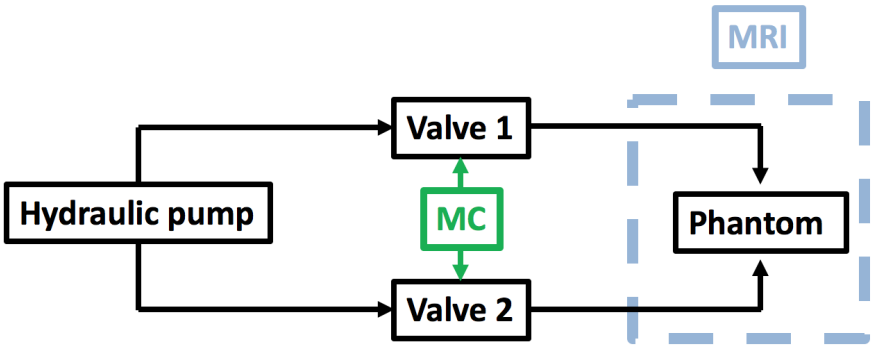

Figure 3.6: Hydraulic system diagram for heart phantom

The phantom's electric control system is presented in Figure 3.7. The activation frequency of the solenoid valves (4) is controlled by a potentiometer (2) and displayed in a 18x2 LCD screen (1). If needed, the same signal that activates the solenoid valves can be used for MRI scan triggering (3). The Arduino code programmed to control the valves is given in Appendix D.

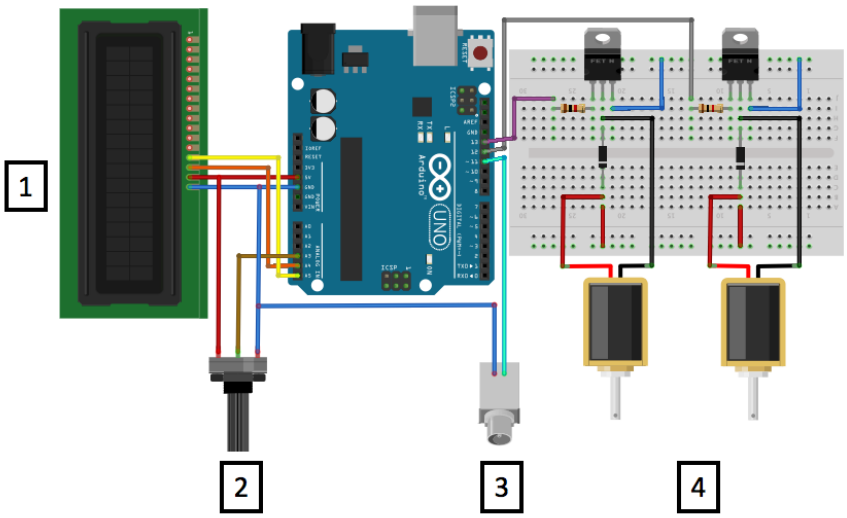

Figure 3.7: Electric design of solenoid valves control.

Measurements for flow, volume, velocity and wall motion were performed for one cardiac cycle to evaluate the fetal heart phantom performance. The measurements were performed four times (n=4) to prove reproducibility. Results for the mentioned tests are presented in Section 4.6.

4 Results

4.1 Simulation of different T2 values with aqueous paramagnetic phantom

Images obtained with SE sequence from different $MnCl_2$ concentration samples are shown in Figure 4.1. Only four of ten echo times (TE) are represented below, nevertheless the signal decay of each sample is visible through each image. The total scan acquisition time for this sequence is 986 s due to the large number of TE.

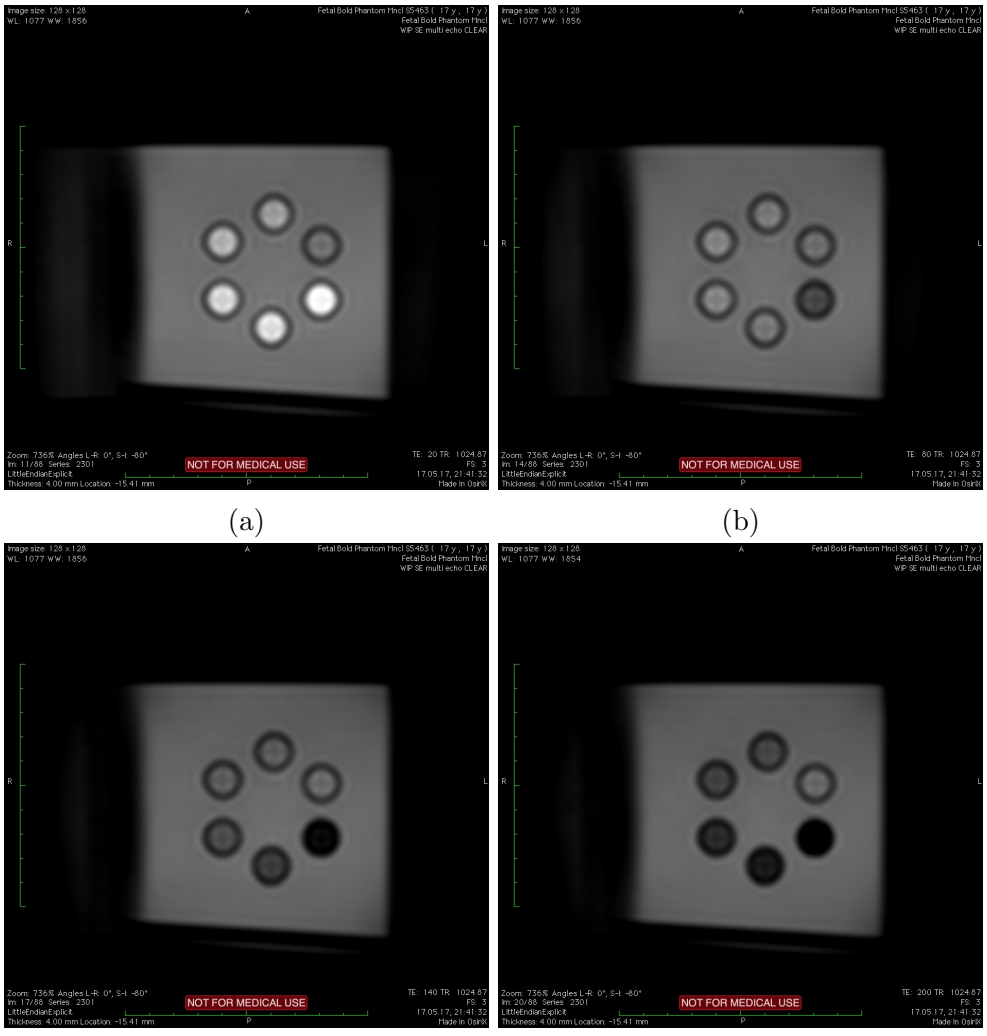

(a) (b)

(c) (d)

Figure 4.1: Signal decay depending on different $MnCl_2$ concentrations obtained with SE sequence. (a) TE=20, (b) TE=80, (c) TE=140, (d)TE=200

Images obtained with BOLD sequence from different $MnCl_2$ concentration samples are shown in Figure 4.2. The decay in signal intensities is clearly visible between each image that represents a different echo time (TE). The total scan acquisition time for this sequence is 61 s for a total of four TE.

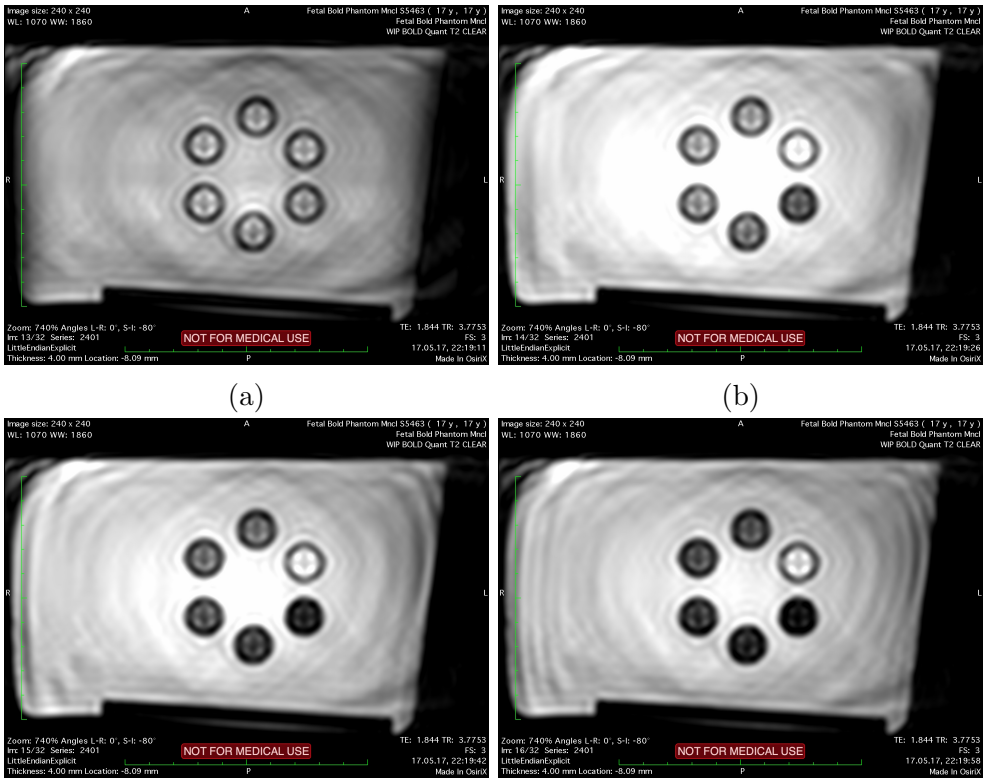

(a) (b)

(c) (d)

Figure 4.2: Signal decay depending on different $MnCl_2$ concentrations obtained with BOLD sequence (a) TE=10, (b) TE=50, (c) TE=100, (d)TE=150

The MRI images appear to present artifacts inside every sample container. Nevertheless, the acquisition of signal intensity values was possible avoiding the artifacts placing the ROI (region of interest) in the inferior-left zone of every container.

The signal intensity values obtained for both sequences were then fitted according to Equation 3.2. As shown in Figure 4.3 SE sequence and BOLD follow an exponential decay.

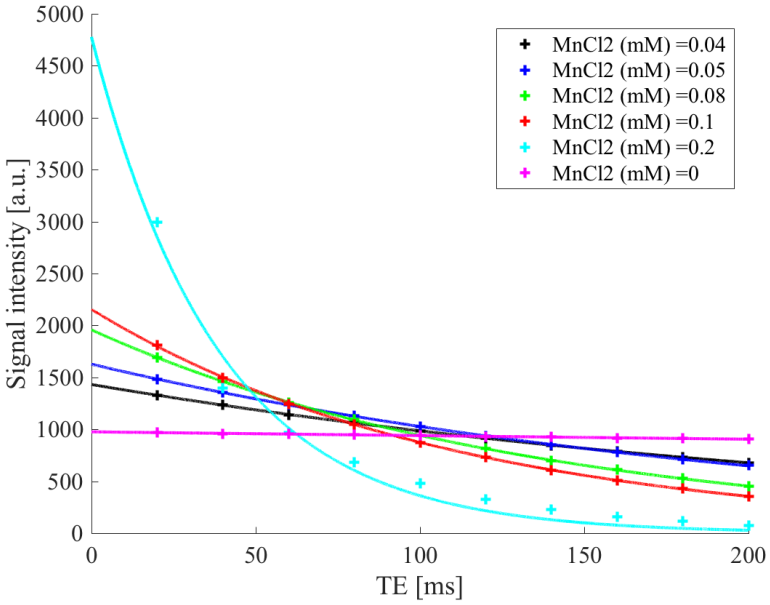

(a)

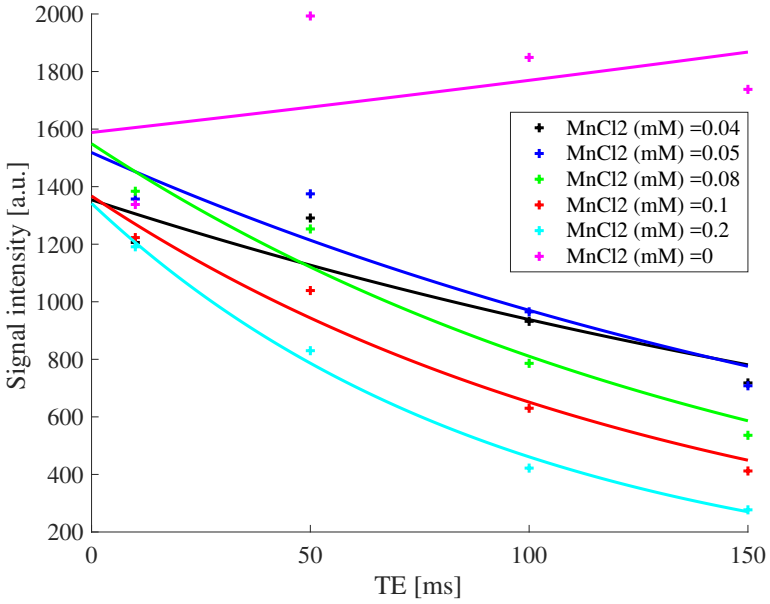

(b)

Figure 4.3: (a) SE sequence, (b) BOLD sequence signal intensity values from different $MnCl_2$ concentrations.

The transverse relaxation values ($T2$) calculated from Equation 3.1 and the measurements obtained by Spin Echo (SE) and BOLD sequences are shown in Table 3.

	Concentration (mM)					
$MnCl_2$	0	0.04	0.05	0.08	0.1	0.2
Type of sequence	**$T2$ value (ms)**					
Equation 3.1	3100	270	220	137	115	34
Spin Echo	2638	267	217	136	110	38
BOLD	925	272	223	154	134	93

Table 3: $T2$ values calculated and obtained by BOLD and SE depending on $MnCl_2$ concentrations

In Figure 4.4 the $T2$ values dependent on $MnCl_2$ concentrations are presented. The $T2$ values from pure water were excluded from the fitting as it presents longer relaxation times.

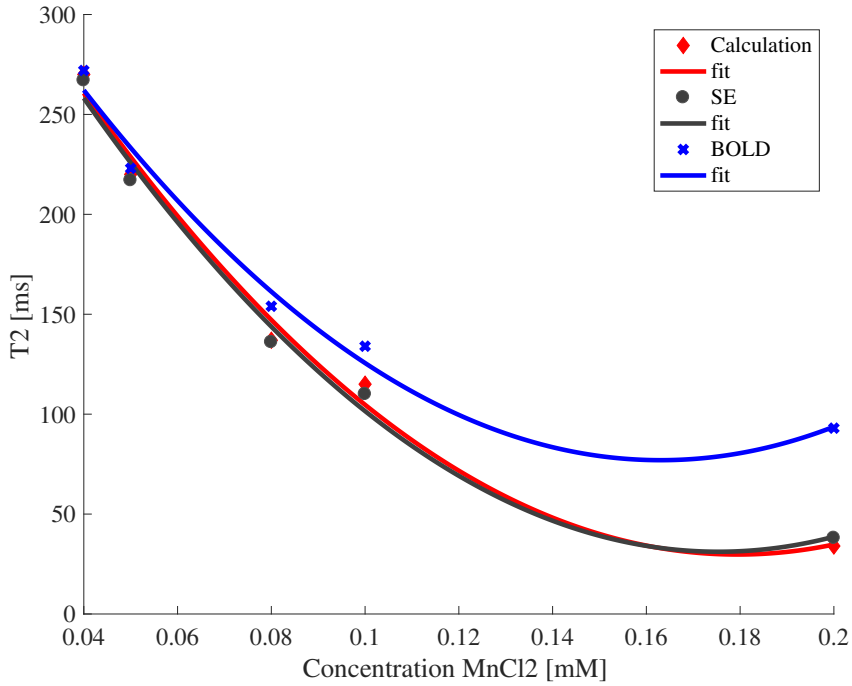

Figure 4.4: T_2 relaxation values depending on $MnCl_2$ concentration obtained on theoretical calculations (red), SE sequence (black), BOLD sequence (blue).

Notice that the graph above shows that the relaxation values for SE and BOLD sequence are similar from 0.04 mM to 0.1 mM, as well as the calculated values with Equation 3.1. A paired t-test was performed to compare both sequences (degrees of freedom= 4, significance level= 0.05, standard error of difference= 9.09). The statistical analysis showed a

P-value= 0.076, indicating that there is no statistically significant difference between the obtained values of both sequences from 0.04 to 0.1 mM. See Appendix C for intermediate values obtained in paired t-test calculation.

The Spin Echo sequences are known for detecting pure $T2$ relaxation, nevertheless the long scanning time does not make it suitable for cardiac imaging [2]. In this tests is proved that a BOLD sequence with acquisition time of 61 s and only four echo times could detect $T2$ relaxation values in a range between 272 ms to 110 ms without any statistical difference compared with a SE sequence with acquisition time of 986 s; thus making the former more appropriate for obtaining $T2$ values in fetal heart examinations.

4.2 Calibration study: Acquisition of coefficients in adult blood (in-vitro)

An example of the images obtained using BOLD sequence in adult blood samples is presented in Figure 4.5, every container shows different signal decay along the echo times. As mentioned in Section 2.6, paramagnetic cells tend to have a faster $T2$ and $T2^*$ decay. Therefore, it is expected that the signal intensity from the samples with lower oxygen values (more paramagnetic) to decay faster.

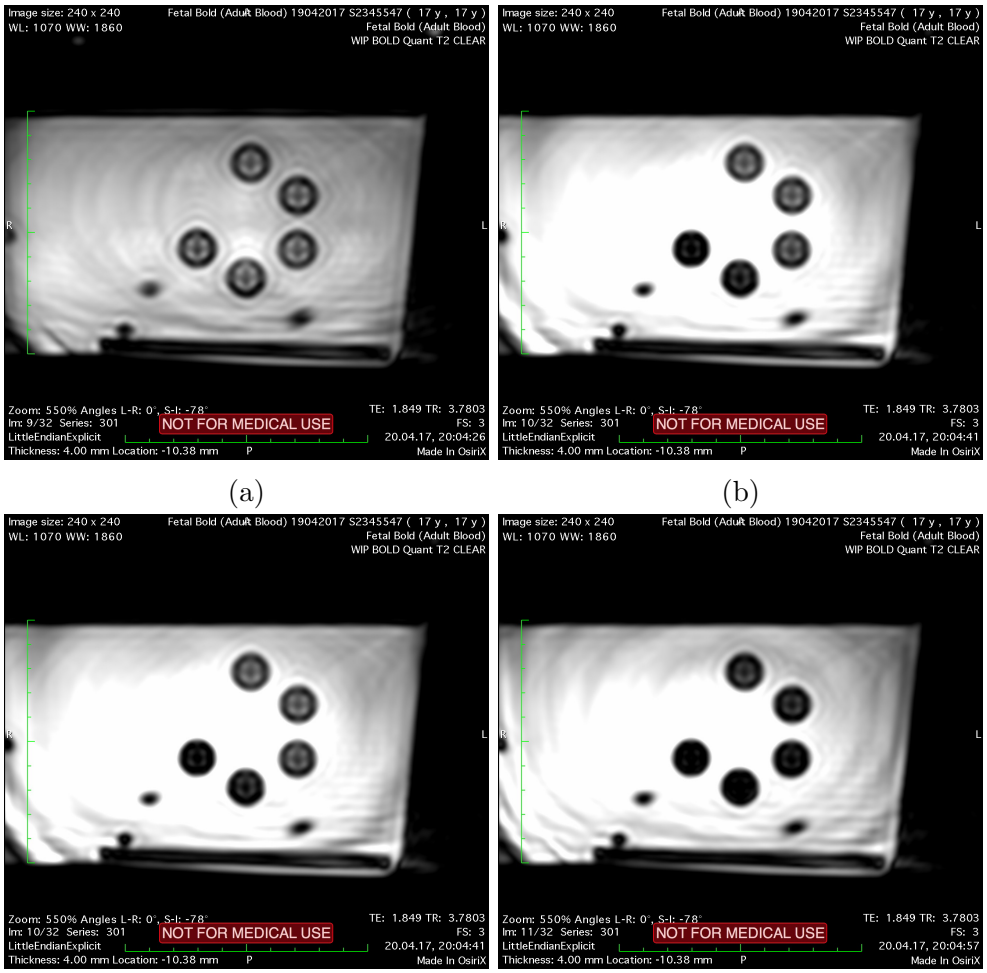

Figure 4.5: Image of adult blood samples with different oxygen values obtained by BOLD sequence in 3T (one slice, different echo times). (a) TE=10, (b)TE=50, (c) TE=100, (d) TE=150.

The oxygen level values obtained before and after the MRI scan are presented in Table 4.

Sample Nr.	1	2	3	4	5	6
Adult 1 (Before)	86	72	61	51	40	18
Adult 1 (After)	89	75	63	54	40	21
Adult 2 (Before)	95	82	70	62	53	-
Adult 2 (After)	97	82	74	63	58	-
Adult 3 (Before)	95	90	83	64	47	-
Adult 3 (After)	96	90	85	70	50	-

Table 4: sO_2 values in adult blood probes.

The blood samples from Adult 1 had to be discarded due to excess of artifacts in MRI scanning. The sample containers for this subject was changed to a smaller volume container to eliminate air bubbles (Monovette 2ml LH, Sarstedt). Despite that, the artifacts were augmented making not possible to measure the signal intensity on these MRI images. Even though the containers provided a effective way to eliminate bubbles, there were not used for the subsequent experiments, replaced by previously used S-Monovette 7.5 ml.

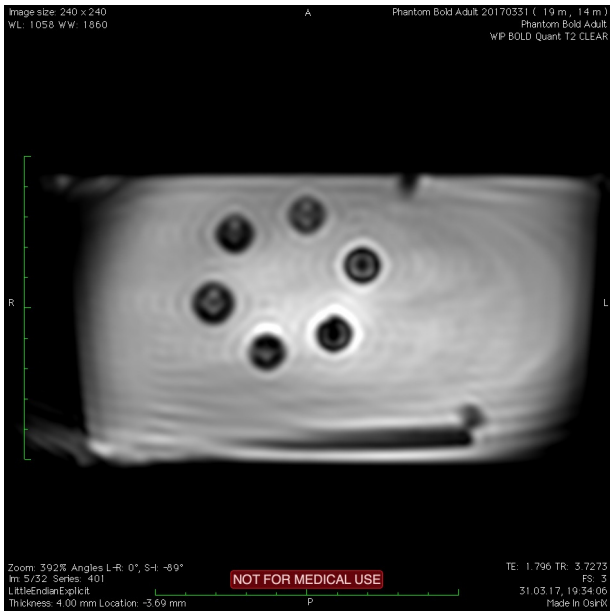

Figure 4.6: Example of blood samples from Adult 1. Presence of augmented artifacts in center of container compared with previous containers.

The paramagnetic effect of low oxygenated blood samples can be observed in Figure 4.7 where the decay rate in the signal intensity curve varies according to the oxygen level. The deoxyhemoglobin in the samples is known to have a high internal magnetization, which causes a higher local field gradient resulting in a faster dephasing of spins and therefore a rapid $T2$ relaxation [50]. In conclusion, the signal decay will be faster depending on how much deoxyhemoglobin a sample has.

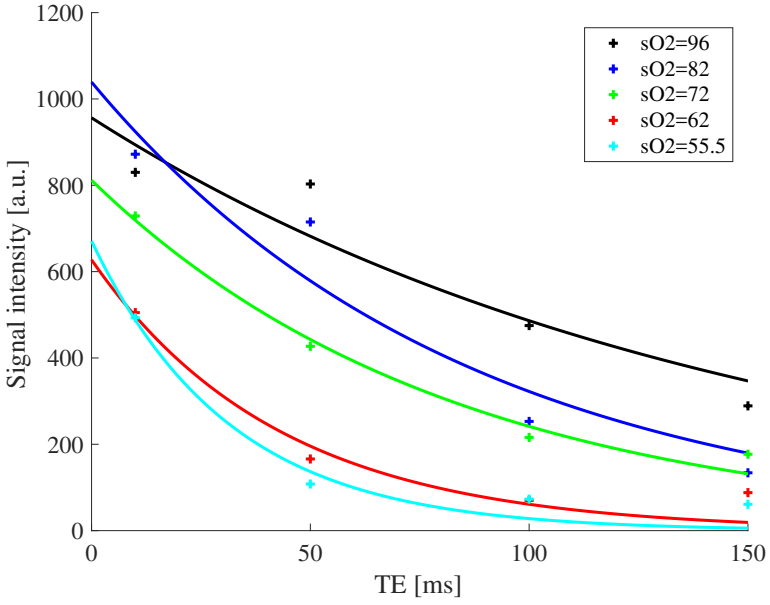

(a)

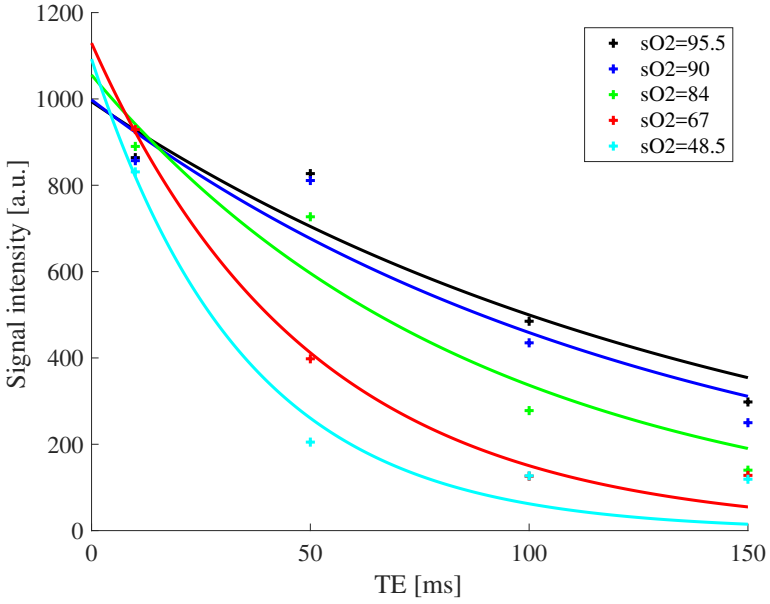

(b)

Figure 4.7: Signal Intensity decay for blood samples in (a) Adult 2, (b) Adult 3.

Subsequently $T2$ relaxation values were calculated based on signal intensity to demonstrate oxygen dependency, as shown in Figure 4.8. The Hct level was considered constant, therefore the calculated $T2$ values for both samples were fitted into a quadratic model that yield three fitting coefficient parameters (a, b, c) which were used to determine the oxygen values in-vivo.

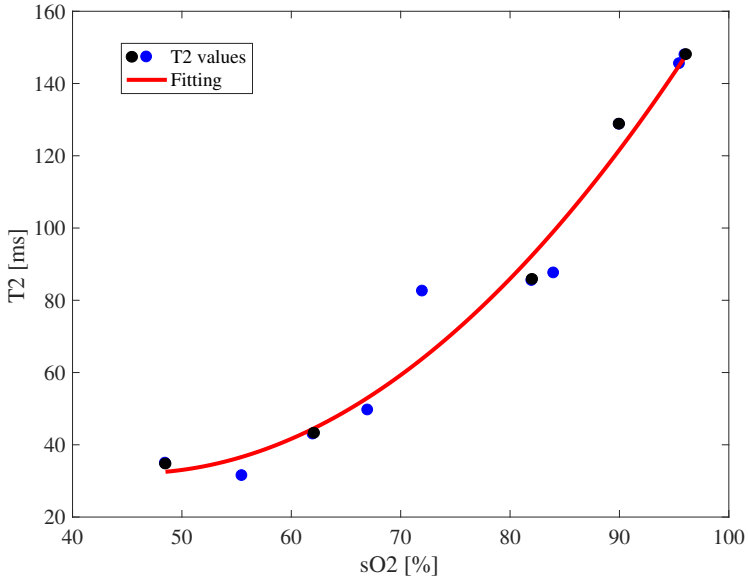

Figure 4.8: $T2$ dependency of sO_2 in vitro for Adult 2 (blue) and Adult 3 (black)

From Equation 3.3, the calculated fitting curve coefficients a,b and c are 0.0052, 0.0265 and 0.0495 respectively. These obtained quantities represent the relationship between hematocrit level, oxygen saturation level and relaxation rate for all samples.

A Pearson's chi-square test was applied to analyze the goodness of fit of the obtained data (degrees of freedom= 9, significance level= 0.05 , X_2crit= 16.95). The statistical analysis showed a X_2= 8.85, indicating that Equation 3.3 has an acceptable fit by compliance of $X_2 << X_2$crit. This assures that the calculated fitting coefficients a,b and c give a good estimation of the model's relationship.

4.3 Validation study: Acquisition of oxygen values in adult blood (in-vivo)

An example of the images obtained using the BOLD sequence in adult heart is presented in Figure 4.9. It is evident that the left ventricle (LV) and right ventricle (RV) show different signal decay along the echo sequences, nevertheless the difference of signal intensities is specially visible in the middle of the sequence (TE=50 and TE=100) in 4.9a and 4.9b.

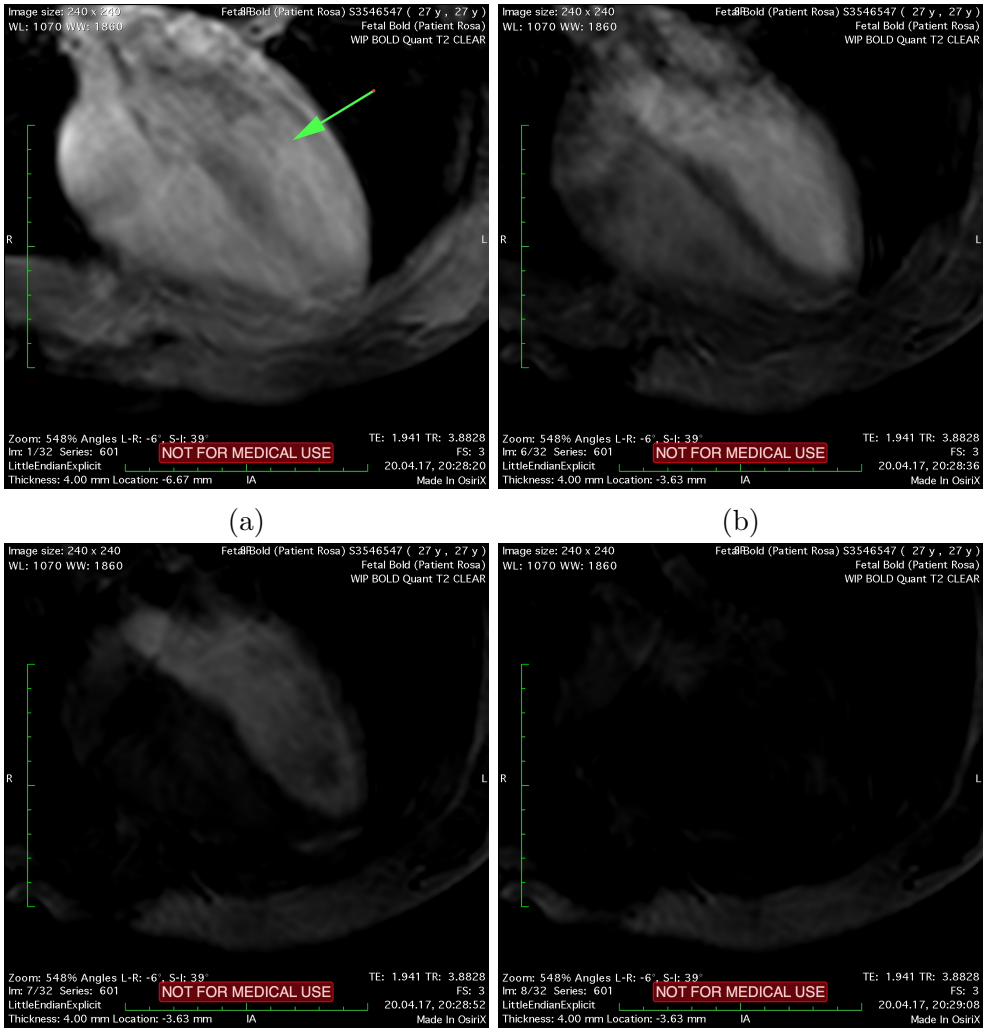

Figure 4.9: Image of adult heart obtained with BOLD sequence in-vivo, green arrow indicates LV. (a) TE=10, (b) TE=50, (c) TE=100, (d) TE=150. No controlled breathing of triggering was used in the performed scan.

.

Signal Intensity values were retrieved from the obtained in-vivo images and a signal decay fitting was performed for both ventricles to calculate $T2$ values using Equation 3.2. The resulting fit for the LV and RV intensities is shown in Figure 4.10a.

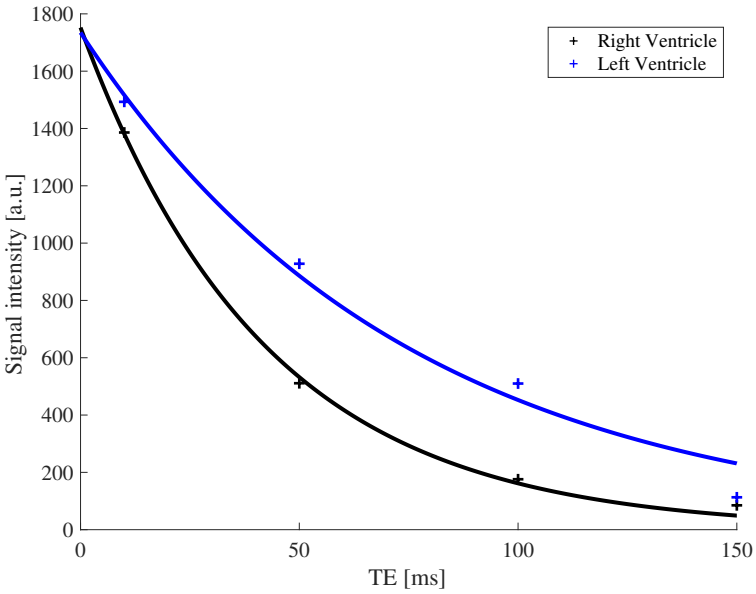

(a)

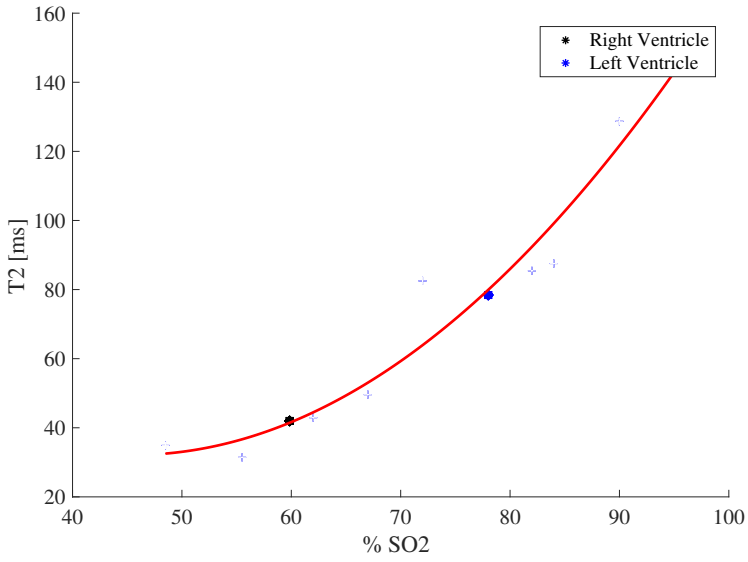

(b)

Figure 4.10: (a) Signal Intensity decay of adult heart obtained in-vivo with BOLD sequence, $T2$ LV= 74.42 ms, $T2$ RV=41.96 ms. (b) Oxygen level calculation for LV and RV in adult heart plotted against calibration curve in-vitro.

Finally, obtained $T2$ values ($T2$ LV= 74.42 ms, $T2$ RV=41.96 ms) and fitting coefficients from Section 4.2 (a=0.0052, b=0.0265 and c=0.0495) were substituted in Equation 3.3.

$$R2 = \frac{1}{T2} = 0.0052 + 0.0265(1 - x) - 0.0495(1 - x)^2 \tag{4.1}$$

Where:

$R2$=Blood relaxation rate (ms^{-1})
$T2$= Blood relaxation time (ms)
x= Saturated oxygen value sO_2 (%)

As shown in Figure 4.10b, the quantitative correlation for the in-vivo $T2$ values resulted in a calculated 78% oxygen level for the left ventricle and 60% for the right ventricle in adult heart. Nevertheless values between 95% to 99% are expected in the LV and 64% to 84% in RV according to literature [1, 18, 20].

4.4 Calibration study: Acquisition of coefficients in fetal blood (in-vitro)

In Figure 4.11 a set of fetal blood scans obtained using BOLD sequence is shown. Each blood sample presents a different signal decay along the four echo times due to the modification of their oxygen level.

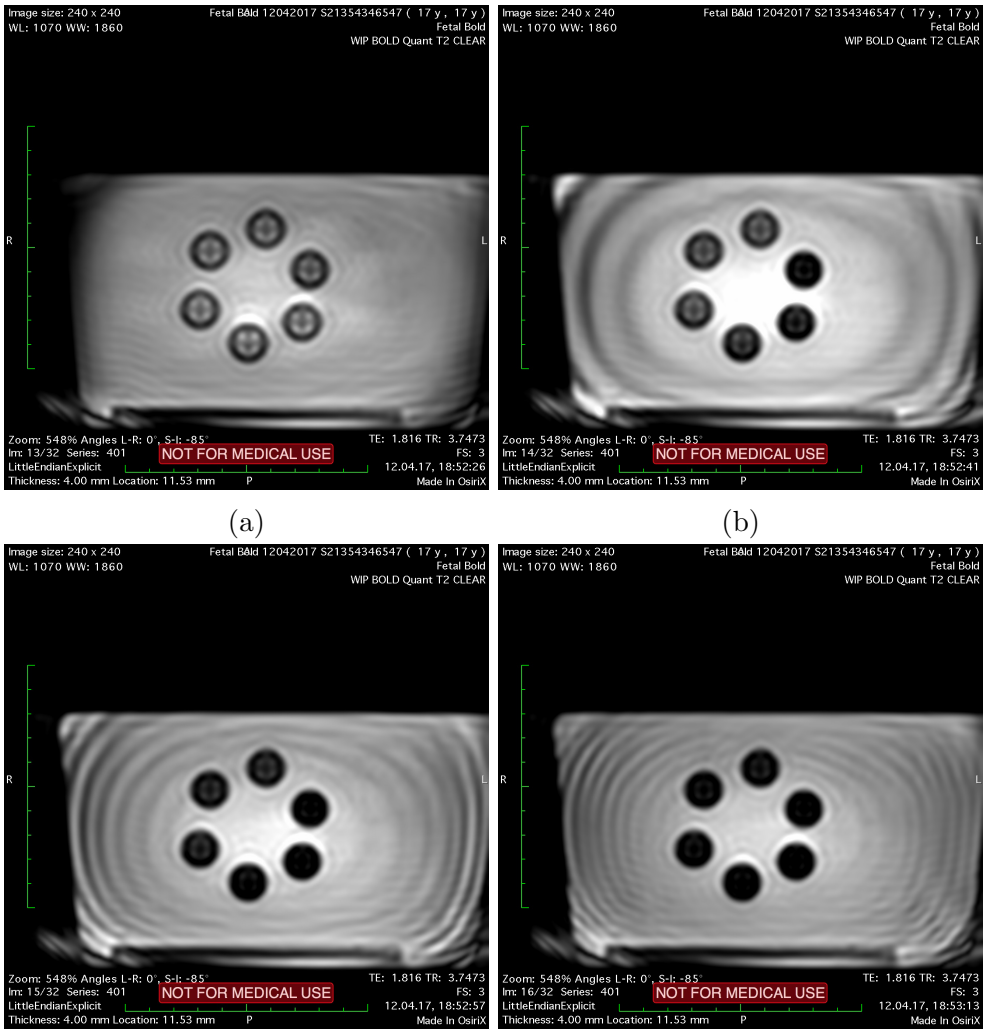

Figure 4.11: Image of fetal blood obtained by BOLD sequence (one slice, different echo times). (a) TE=10, (b) TE=50, (c) TE=100, (d) TE=150.

The oxygen level values of the fetal blood samples measured before and after the MRI scan are presented in Table 5.

Sample Nr.	1	2	3	4	5	6
Fetal 1 (Before)	96	89	83	68	56	42
Fetal 1 (After)	97	90	89	80	71	55
Fetal 2 (Before)	92	82	60	55	40	-
Fetal 2 (After)	96	93	70	58	54	-

Table 5: sO_2 values in fetal blood probes.

Signal Intensity decay curve for fetal blood samples is shown in Figure 4.12. The deoxyhemoglobin effect can be observed between the fetal blood samples as the signal decay rate varies in each TE. As expected, the samples with lower sO_2 values have a faster signal decay. It can also be noticed that in TE=50 the signal intensities present a non-exponential behavior in comparison to the other values.

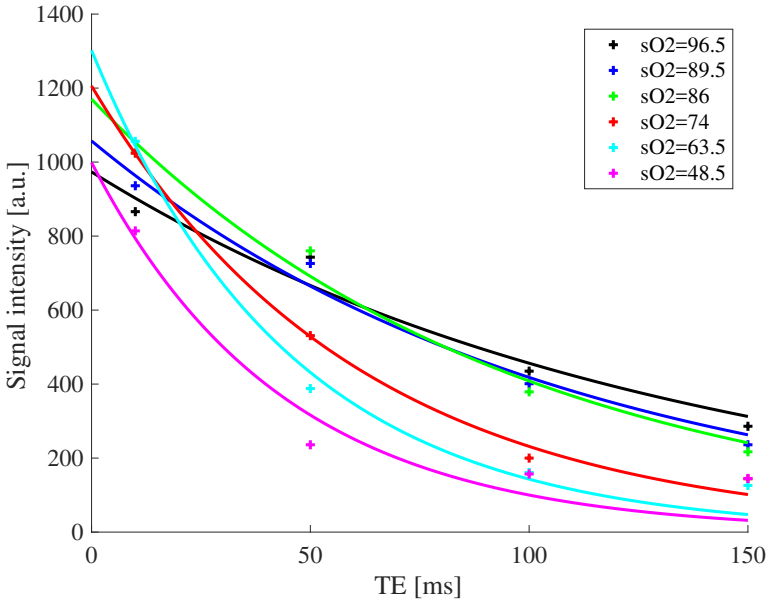

(a)

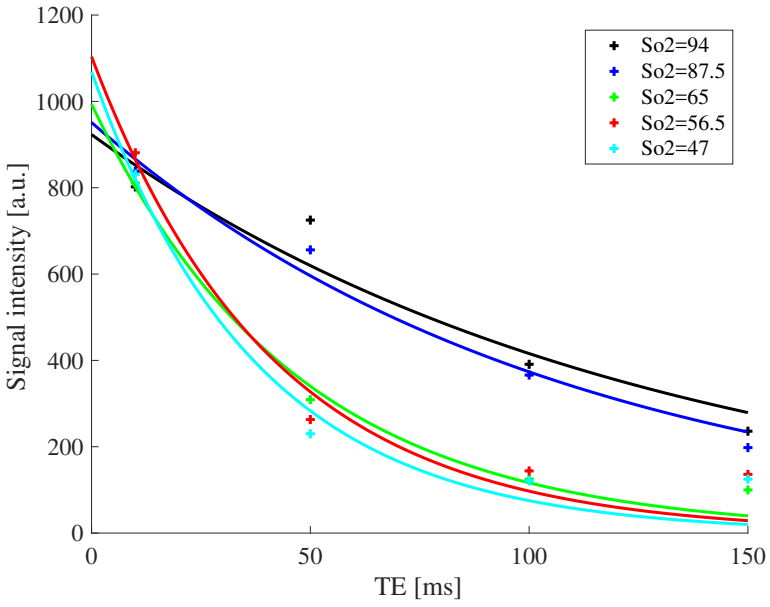

(b)

Figure 4.12: Signal Intensity decay for fetal blood samples. (a) Fetal subject 1, (b) Fetal subject 2

Signal decay equation 3.2 was used to calculate $T2$ values from the previously obtained signal intensities of each sample. Subsequently, resulting $T2$ values from both samples where fitted by Equation 3.3 to determine coefficients a, b and c as shown in Figure 4.13.

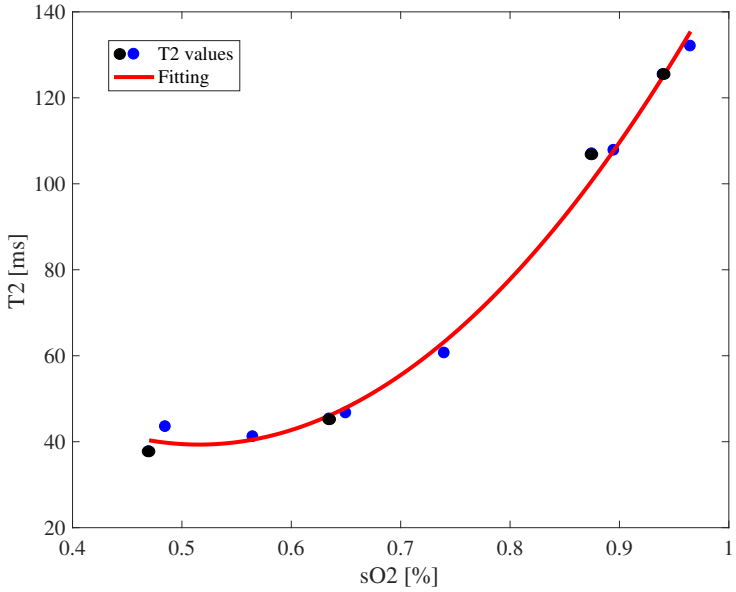

Figure 4.13: $T2$ dependency of oxygen levels in vitro for Fetal 1 (blue) and Fetal 2 (black) samples.

The following fitting coefficients were obtained for fetal probes: a=0.0041, b=0.058, c=-0.0333. These coefficients would be implemented for the in-vivo oxygen quantification.

A Pearson's chi-square test was performed to determine the goodness of fit for the obtained coefficients (degrees of freedom= 10, significance level= 0.05, X_2crit= 18.31). The statistical analysis showed a X_2= 4.2, indicating that Equation 3.3 has an acceptable fit by compliance of $X_2 << X_2$crit. This assures that the calculated fitting coefficients a,b and c provide an adequate estimation of the model relationship.

4.5 Validation study: Acquisition of oxygen values in fetal blood (in-vivo)

An example of the images obtained using BOLD sequence in a 32 week healthy fetus is presented in Figure 4.14. The small size and rapid movement of the fetal heart represents a challenge in the MRI modality, nevertheless it was possible to perform the scan without cardiac triggering. It was chosen to analyze the left ventricle only, as it is expected to contain a higher oxygen concentration and therefore a slower $T2$ decay that can be easily detected by the developed sequence.

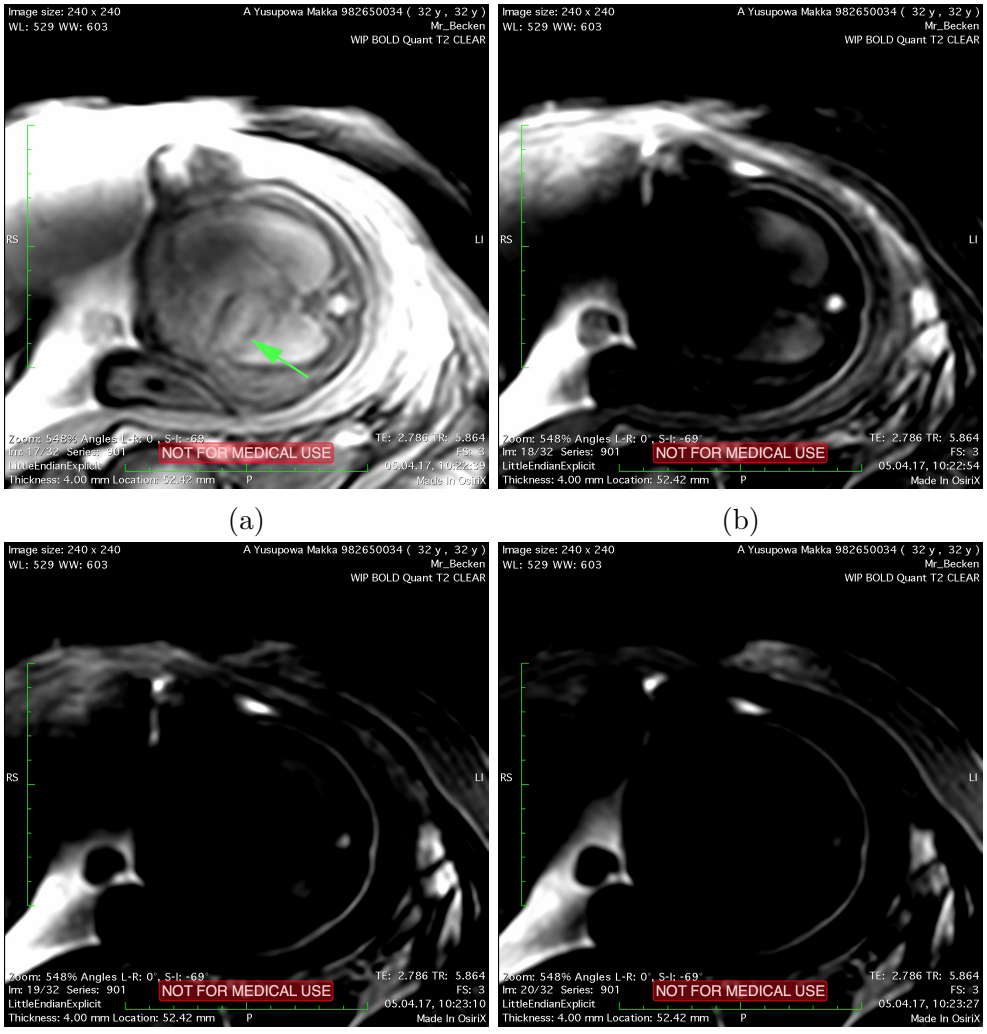

Figure 4.14: Image of a fetal heart obtained with BOLD sequence in vivo, green arrow indicates the left ventricle. (a) TE=10, (b) TE=50, (c) TE=100, (d)TE=150. Mother controlled breathing and no triggering where used in the scans.

Signal intensity values were retrieved from the obtained in-vivo scans in the left ventricle. Afterwards, a signal decay fitting was performed to calculate $T2$ value using Equation 3.2. The obtained fit is shown in Figure 4.15a.

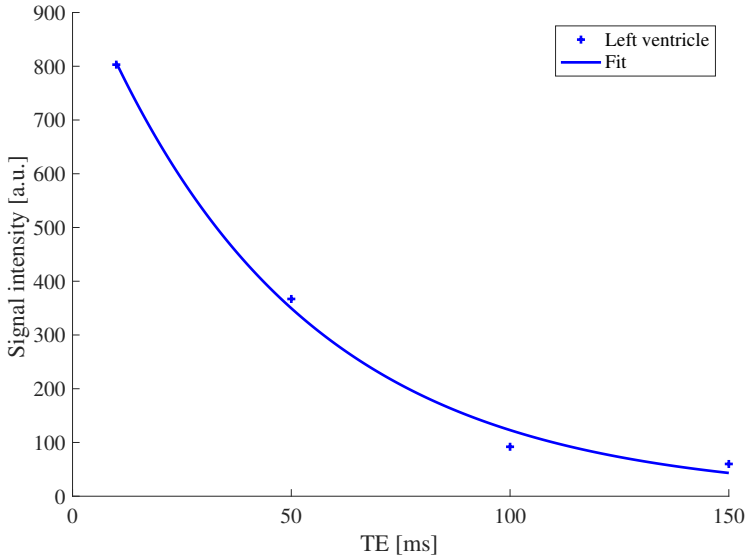

(a)

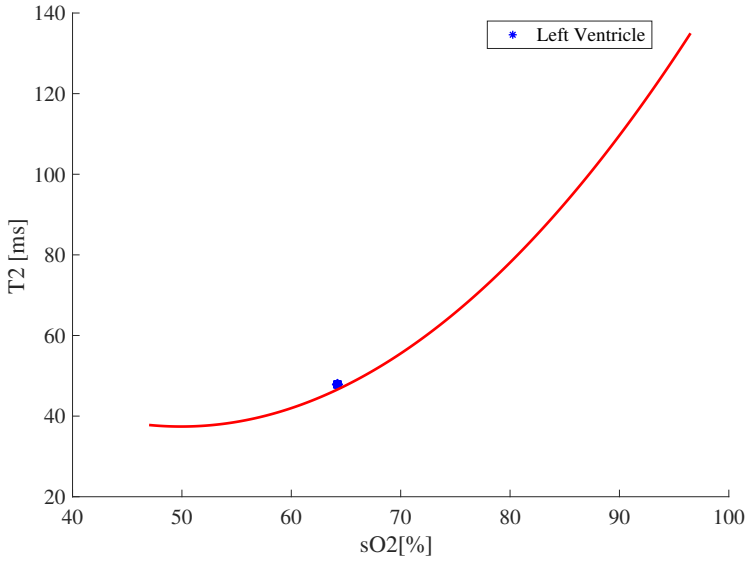

(b)

Figure 4.15: (a) Signal Intensity decay of fetal heart obtained in-vivo with BOLD sequence, $T2$ LV= 47.8 ms. (b) Oxygen level calculation for LV in fetal heart plotted against calibration curve in-vitro.

The fitted $T2$ value ($T2$ LV= 47.8 ms) for the in-vivo measurement and the fitting coefficients obtained in Section 4.2 (a=0.0041, b=0.058 and c=-0.0333) were substituted to solve Equation 3.3.

$$R2 = \frac{1}{T2} = 0.0041 + 0.058(1-x) - 0.033(1-x)^2 \tag{4.2}$$

Where:

$R2$=Blood relaxation rate (ms^{-1})
$T2$= Blood relaxation time (ms)
x= Saturated oxygen value sO_2 (%)

The quantitative correlation for the in-vivo $T2$ values resulted in a calculated 64% oxygen level for the left ventricle in the fetal heart. The fitting curve and resulting correlation can be observed in Figure 4.15b.

In a similar study performed by Wedegaertner et al., a catheter was placed surgically in the right carotid artery of sheep fetus to measure directly the sO_2 values. This catheter indicated an oxygenation mean value of 70% [49]. This value is found to be slightly higher compared with the 64% saturation level calculated by the fetal validation study in this work.

Finally a comparison between the obtained dependence from fetal blood and adult blood is shown in Figure 4.16. It can be noticed that at lower oxygen values, fetal blood presents higher $T2$ values and as oxygen increases adult blood $T2$ changes at faster rate.

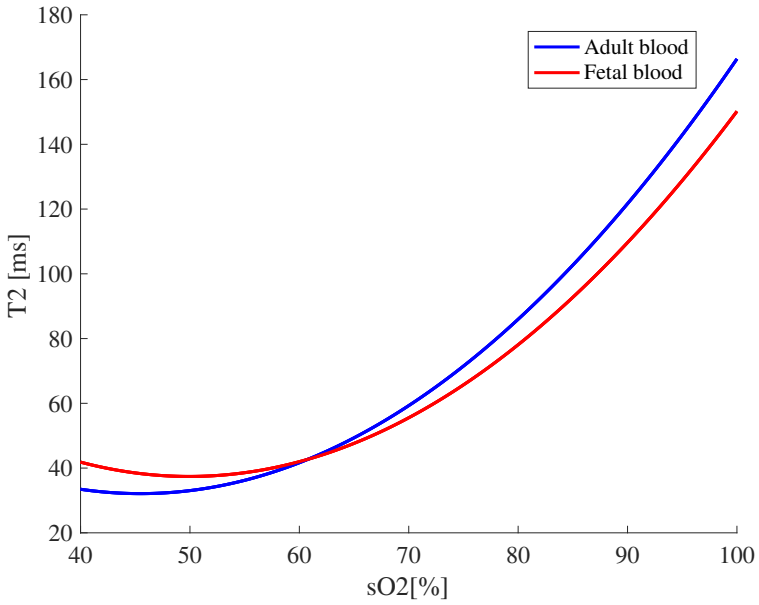

Figure 4.16: Dependence of fetal blood $T2$ on sO_2 is different that from adult blood $T2$ at hct=0.44.

4.6 Simulation of cardiac volume, flow and velocity in fetal heart

4.6.1 Cardiac volume in phantom

The volume over one cardiac cycle was measured in the left ventricle. As Figure 4.17a shows, it is evident that as the heart starts to fill (diastole phase), a volume increment is presented. On the other hand, in the contraction (systole phase), the phantom ejects the water staying with a residual volume of 2 ml. The result for maximal volume on the phantom's left ventricle is 5.3 ml (±0.4) compared with 7.7 ml (±1.4) in a real 37 weeks fetal heart [30].

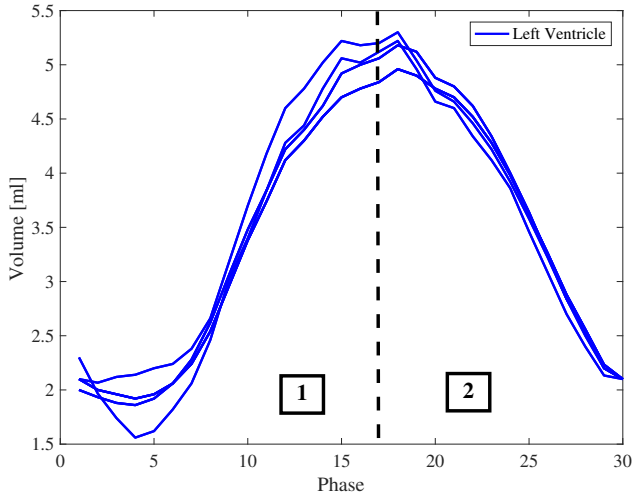

(a)

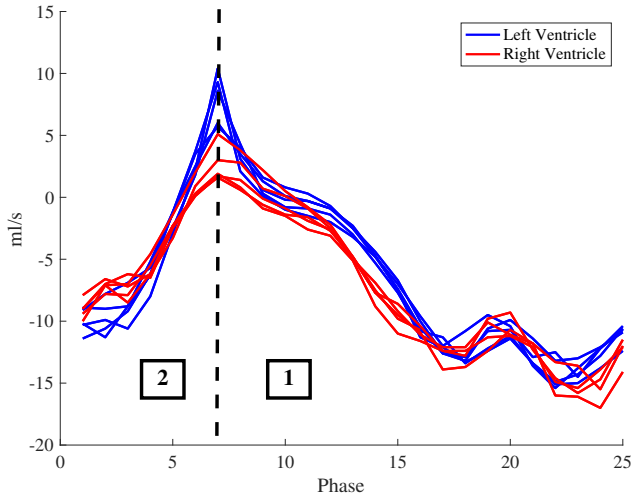

(b)

Figure 4.17: (a)Volume measured in the left ventricle. Diastole phase (1), systole phase (2), (b) Flow measured in output ventricles. Diastole phase (1), systole phase (2).

4.6.2 Cardiac flow in phantom

Pulsatile flow was measured in both left and right ventricle outputs in fetal phantom. Figure 4.17b shows that in systole, the phantom reaches an average maximum flow of 8.6 ml/s (±3.1) compared with real values of 17.1 ml/s(±1.4) [30].

4.6.3 Cardiac velocity in phantom

Flow velocity was measured in both left and right ventricle outputs in fetal phantom. Figure 4.18 shows that is systole, the phantom reaches an average maximum velocity of 33.7 cm/s (±4.1) simulating the in-vivo values of 32 cm/s (±0.2) [30].

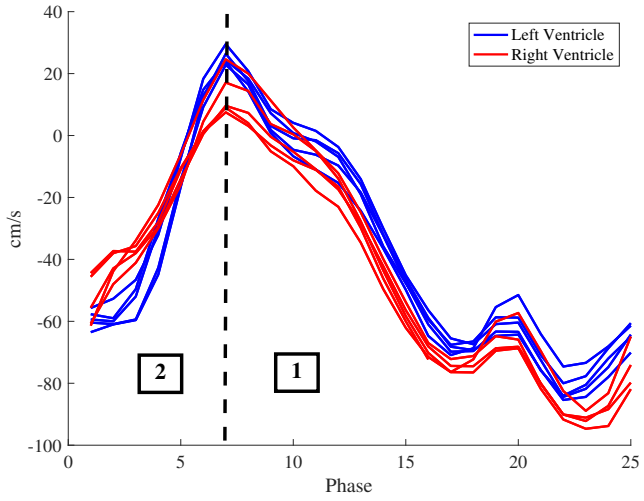

Figure 4.18: Velocity measured in output ventricles. Diastole phase (1), systole phase (2)

5 Discussion

For all blood calibration studies in section 3.3 "Calibration study: Acquisition of coefficients in adult blood" and section 3.5 "Calibration study: Acquisition of coefficients in fetal blood", sodium dithionite was added to the blood probes for deoxygenation. Saebo et al. demonstrated that using a small concentration (2.5 mg/g blood) does not affect the structure and function of the cell membrane [5], thus not affecting the relaxation rates of the BOLD measurements.

In section 4.6 "Simulation of cardiac volume, flow and velocity in fetal heart" a difference in flow values between in-vivo and the phantom is presented. This is caused by the distinct diameter measurements of the fetal aorta (6-8 mm) [9] compared with the simulated arteries in the phantom (12 mm). Additionally, negative flow and velocity values in the diastole, indicate that the heart presents back-flow, i.e. when the heart expands, the already ejected water returns to the phantom's ventricles. Testing using the created fetal heart phantom is required to examine the impact of flow in the study and quantify the potential variation of data.

Several factors were identified that could have influenced the obtained results in this study:

In section 3.3.4 "Calculation of fitting parameters", hematocrit level was assumed constant for all samples. Nevertheless, paramagnetization is induced by an hemoglobin state and is contained in red blood cells. Therefore the red blood cells' amount, i.e hematocrit, affects the local field gradients, which in turn affect the $T2$ relaxation times. Further experiments are necessary to quantify the $T2$-oxygen relationship with different hematocrit values.

Imaging artifacts where present in calibration probes from sections 3.3 "Calibration study: Acquisition of coefficients in adult blood" and section 3.5 "Calibration study: Acquisition of coefficients in fetal blood". They were identified as Gibbs' or truncation artifacts, which occur when high-contrast interfaces are present (container/blood in this work) and could have affected the posterior signal intensity analysis. Fourier transforms are used to reconstruct MR signals into images, but with a restricted sampling the Fourier series has to be truncated. This truncation results in significant artifacts when a high-contrast interface is presented [3, 12]. Furthermore, to minimize this error the number of phase-encode steps has to be increased in the sequence.

As observed through the calibration studies, and as shown in Figure 5.1a the signal intensities for TE=50 lay always above the exponential fitting curve. This effect may be attributed to the short time interval between pulse elements that does not allow the complete relaxation on the transverse plane.

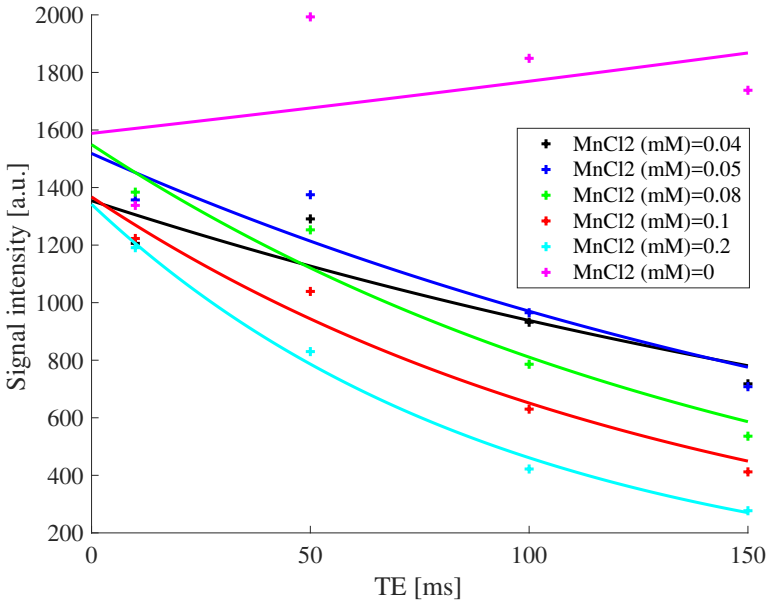

(a)

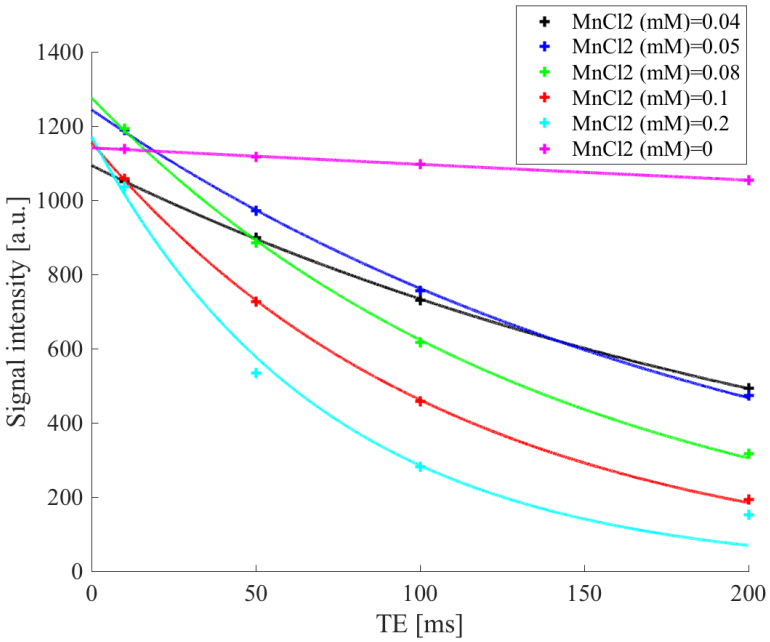

(b)

Figure 5.1: (a) Original BOLD sequence (b) Modified sequence: half flip angle, delay=10000 ms between pulses.

This issue was corrected in the sequence by lowering the flip angle value to allow a rapid relaxation and adding a long delay (10 s) between each echo pulse to prevent energy accumulation from the previous pulse, as shown in Figure 5.1b.

In the study performed by Wedegaertner et al. [49], the BOLD sequence was triggered by the mother sheep's respiration, in comparison to only breathing controlled and non-triggered method applied. This would mean that the developed sequence is affected by the respiration movement and following studies must be carried out with a respiration triggering method.

As stated in section 3.2 "Simulation of different $T2$ values with aqueous paramagnetic phantom" the developed BOLD sequence presents no statistical difference compared with a SE sequence in the range from 272 ms - 110 ms, which means the acquisition of pure $T2$ values by BOLD. Nevertheless it can be speculated that outside this range of values, the BOLD signal intensities are influenced by other factors such as residual longitudinal magnetization which will cause $T1$ weighting and background signal.

6 Conclusion and Outlook

The completion of this project signifies the successful quantification of the dependency between neonatal blood relaxation ($T2$) and oxygen saturation levels (sO_2) which was applied afterwards to determine sO_2 values in MRI fetal cardiac imaging.

The achieved results yield a clear quadratic relationship between $T2$ and sO_2 obtained by a blood oxygen level dependent sequence (BOLD), demonstrating that a non-invasive estimation of fetal oxygenation is feasible through an in-vitro calibration method.

For the practical application of this method, further analysis must be performed including simulations with reproducible flow patterns in heart phantom to measure the precise flow effects on BOLD, and mother respiratory triggering in in-vivo measurements to reduce scanning noise. Such actions will increase the model's accuracy, giving a broader knowledge of the flow and movement effects in the sequence.

Improvements in the actual sequence must be made to correct the quantification between each pulse and eliminate remaining longitudinal magnetization. A long delay between echo pulses was used in this case, however is not recommended for the in-vivo validation studies. It is suggested to implement a rapid flow saturation pre-pulse at the beginning of each interval to prevent the accumulation of longitudinal magnetization and signal disturbances caused by cardiac flow in future tests.

As there are only a small number of studies in the fetal BOLD field, the quantification of this dependency is expected to support further research in the application of BOLD sequences in fetal blood oxygenation measurements, facilitating the detection of abnormal oxygen supply in the gestational period and preventing its consequences.

A Fitting parameter and oxygen calculation code

```
%%%%%%%%%%%%%%%%%%%%%%%%%%%%%%%%%%%%%%%%%%%%%%%%%%%%%%%%%%%%%%%%
% Program to calculate oxygen level in-vitro
% INPUT: a,b,c parameters of BOLD_Calibration
% OUTPUT: % of Oxygen Saturation
% Author: Rosa Ortiz
% Master Thesis HAW in cooperation with UKE
%%%%%%%%%%%%%%%%%%%%%%%%%%%%%%%%%%%%%%%%%%%%%%%%%%%%%%%%%%%%%%%%

 %% Load data
 close all
 clear all

 M_data= xlsread('Signal_Fetal_1');
 [data.rows,data.columns]=size(M_data);
 TF=isnan(M_data);

 for i=1:data.rows
         if TF(i,1)== 0
                 data.echos(i,1)=M_data(i,1);
         end
 end

 for i=2:data.columns
         for j=1:data.rows-2
                 data.signal(j,i-1)=M_data(j,i);
         end
 end

 data.o2_measured=M_data(data.rows,2:data.columns)';
 data.o2_measured= data.o2_measured./100;
 [data.Nr_of_tests,n]=size(data.o2_measured);
 [data.nr_echos,n]=size(data.echos);

 %% T2 calculation and plotting

 if data.Nr_of_tests==5
         ft = fittype('exp_fit(x,S0,R2)');

         fit1= fit(data.echos,data.signal(:,1),ft,'StartPoint'
             ,[0,0]); %x=data.echos y=data.signal
         fit2= fit(data.echos,data.signal(:,2),ft,'StartPoint'
             ,[0,0]);
```

```
42          fit3= fit(data.echos,data.signal(:,3),ft,'StartPoint'
                ,[0,0]);
43          fit4= fit(data.echos,data.signal(:,4),ft,'StartPoint'
                ,[0,0]);
44          fit5= fit(data.echos,data.signal(:,5),ft,'StartPoint'
                ,[0,0]);
45          data.R2= [fit1.R2; fit2.R2; fit3.R2; fit4.R2; fit5.R2];
46          data.T2= 1./data.R2;
47          data.R2=data.R2;
48
49          plotx= 0:0.001:data.echos(data.nr_echos,1);
50          ploty=[fit1(plotx) fit2(plotx) fit3(plotx) fit4(plotx)
                fit5(plotx)];
51
52          figure(1)
53          hold on
54                  for i=1:data.Nr_of_tests
55                  plotStyle={'k','b','g','r','c'};
56                  plot(plotx,ploty(:,i),plotStyle{i},'LineWidth'
                        ,2)
57
58                  plotStyle={'k+','b+','g+','r+','c+'};
59                  plot(data.echos,data.signal(:,i),plotStyle{i},'
                        LineWidth',2)
60
61                  xlabel('TE [ms]')
62                  ylabel('Signal intensity [a.u.]')
63                  title('BOLD SEQUENCE')
64                  legendInfo{i}=['% SO2=',num2str(data.o2_measured
                        (i,1))];
65                  set(gca, 'FontName', 'Times','FontSize',16,'
                        FontWeight','normal')
66  end
67
68          h=zeros(5,1);
69          h(1)=plot(NaN,NaN,'k+','LineWidth',2);
70          h(2)=plot(NaN,NaN,'b+','LineWidth',2);
71          h(3)=plot(NaN,NaN,'g+','LineWidth',2);
72          h(4)=plot(NaN,NaN,'r+','LineWidth',2);
73          h(5)=plot(NaN,NaN,'c+','LineWidth',2);
74
75  legend(h,legendInfo,'% sO2')
76  hold off
77
78 end
```

```
79
80  if data.Nr_of_tests==6
81          ft = fittype('exp_fit(x,S0,R2)');
82          fit1= fit(data.echos,data.signal(:,1),ft,'StartPoint'
                ,[0,0]);
83          fit2= fit(data.echos,data.signal(:,2),ft,'StartPoint'
                ,[0,0]);
84          fit3= fit(data.echos,data.signal(:,3),ft,'StartPoint'
                ,[0,0]);
85          fit4= fit(data.echos,data.signal(:,4),ft,'StartPoint'
                ,[0,0]);
86          fit5= fit(data.echos,data.signal(:,5),ft,'StartPoint'
                ,[0,0]);
87          fit6= fit(data.echos,data.signal(:,6),ft,'StartPoint'
                ,[0,0]);
88          data.R2= [fit1.R2; fit2.R2; fit3.R2; fit4.R2; fit5.R2;
                fit6.R2 ];
89          data.T2=1./data.R2;
90          plotx= 0:0.01:data.echos(data.nr_echos,1);
91          ploty=[fit1(plotx) fit2(plotx) fit3(plotx) fit4(plotx)
                fit5(plotx) fit6(plotx)];
92
93
94          figure(1)
95          hold on
96                  for i=1:data.Nr_of_tests
97
98                          plotStyle={'k','b','g','r','c','m'};
99                          plot(plotx,ploty(:,i),plotStyle{i},'
                               LineWidth',2)
100                         plotStyle={'k+','b+','g+','r+','c+','m+'
                               };
101                         plot(data.echos,data.signal(:,i),
                               plotStyle{i},'LineWidth',2)
102
103                         xlabel('TE [ms]')
104                         ylabel('Signal intensity [a.u.]')
105                         title('BOLD SEQUENCE')
106                         legendInfo{i}=['%SO2=',num2str(data.
                               o2_measured(i,1))];
107                         set(gca, 'FontName', 'Times','FontSize'
                               ,16,'FontWeight','normal')
108
109                 end
110
```

```
111 h=zeros(6,1);
112 h(1)=plot(NaN,NaN,'k+','LineWidth',2);
113 h(2)=plot(NaN,NaN,'b+','LineWidth',2);
114 h(3)=plot(NaN,NaN,'g+','LineWidth',2);
115 h(4)=plot(NaN,NaN,'r+','LineWidth',2);
116 h(5)=plot(NaN,NaN,'c+','LineWidth',2);
117 h(6)=plot(NaN,NaN,'m+','LineWidth',2);
118
119 legend(h,legendInfo,'%SO2')
120 hold off
121
122 end
123
124 %% Calculation of fitting coefficients
125
126 ft= fittype('cuad_fit(x,a,b,c)');
127 Fits_SO2=fit(data.o2_measured,data.R2,ft,'StartPoint',[0,0,0]);
128 data.A=Fits_SO2.a;
129 data.B=Fits_SO2.b;
130 data.C=Fits_SO2.c;
131
132
133 figure(2)
134 Fits_T2=fit(data.o2_measured,data.T2,ft,'StartPoint',[0,0,0]);
135
136 plot(Fits_T2,data.o2_measured,data.T2,'b+')
137 legend ('T2 values','Fitting')
138 xlabel('sO2')
139 ylabel('T2 [ms]')
140 title('BOLD SEQUENCE)
141 %set(gca, 'FontName', 'Times','FontSize',16,'FontWeight','
      normal')
142
143
144 %% Calculation of SO2 values (validation of method)
145
146 data.mat=[data.A data.B data.C];
147 syms R2 x a b c
148 f= solve('a + b*(1-x) + c*(1-x)^2-R2',x);
149 fun=@(R2,a,b,c) (b + 2*c - (b^2 + 4*R2*c - 4*a*c)^(1/2))/(2*c);
150
151 for i=1:data.Nr_of_tests
152 data.calculated_o2(i,1)=abs(fun(data.R2(i,1),data.mat(1),data.
      mat(2),data.mat(3)));
153 end
```

```
%%%%%%%%%%%%%%%%%%%%%%%%%%%%%%%%%%%%%%%%%%%%%%%%%%%%%%%%%%%%%
% Program to calculate oxygen level in-vivo
% INPUT: a,b,c parameters of BOLD_Calibration
% OUTPUT: % of Oxygen Saturation
% Author: Rosa Ortiz
% Master Thesis HAW in cooperation with UKE
%%%%%%%%%%%%%%%%%%%%%%%%%%%%%%%%%%%%%%%%%%%%%%%%%%%%%%%%%%%%%

 %% Load data

 M_BOLD= xlsread('Signal_Fetal_InVivo');
 [bold.rows,bold.columns]=size(M_BOLD);
 TF=isnan(M_BOLD);

 for i=1:bold.rows
        if TF(i,1)== 0
                bold.echos(i,1)=M_BOLD(i,1);
        end

 end

 for i=2:bold.columns
        for j=1:bold.rows
                 bold.signal(j,i-1)=M_BOLD(j,i);
         end
 end

 bold.Nr_of_tests=bold.columns-1;



 if bold.Nr_of_tests==1
        ft = fittype('exp_fit(x,S0,R2)');
        fit1b= fit(bold.echos,bold.signal(:,1),ft,'StartPoint',[0,0]); %x=data.echos y=data.signal
        bold.R2= fit1b.R2;
         bold.T2= 1./bold.R2;
end

 figure(3)
 hold on
        plot(fit1b,bold.echos,bold.signal,'+k')
        set(gca, 'FontName', 'Times','FontSize',16,'FontWeight','normal')
```

```
44          xlabel('TE [ms]')
45          ylabel('Signal intensity [a.u.]')
46
47  hold off
48
49
50  fun=@(R2,a,b,c) (b + 2*c - (b^2 + 4*R2*c - 4*a*c)^(1/2))/(2*c);
51
52  for i=1:bold.Nr_of_tests
53          bold.calculated_o2(i,1)=fun(bold.R2(i,1),data.mat(1),
                data.mat(2),data.mat(3));
54  end
55
56
57  figure(4)
58  legendInfo={'Left Ventricle'};
59
60  hold on
61          set(gca, 'FontName', 'Times','FontSize',16,'FontWeight',
                'normal')
62          plot(bold.calculated_o2(1,:),bold.T2(1,:),'b*')
63          plot(Fits_T2,data.o2_measured,data.T2)
64          h=zeros(2,1);
65          h(1)=plot(NaN,NaN,'b*','LineWidth',1);
66          h(2)=plot(NaN,NaN,'b*','LineWidth',2);
67          legend(h,legendInfo)
68          xlabel('sO2[%] ')
69          ylabel('T2 [ms]')
70          title('BOLD sequence')
71  hold off
```

B Chi-square goodness of fit code

```
%%%%%%%%%%%%%%%%%%%%%%%%%%%%%%%%%%%%%%%%%%%%%%%%%%%%%%%%%%%%%
% Program to calculate the chi-square goodness of fit.
% Is sample data consistent with found distribution?
% NOTE: Run BOLD_Calibration.mat to obtain values
%
% INPUT:   1. Observed: T2 values obtained from MRI BOLD scan
%          2. Expected: T2 values calculated in the fitting
% Output: Chi squared value
% Author: Rosa Ortiz
% Master Thesis HAW in cooperation with UKE
%%%%%%%%%%%%%%%%%%%%%%%%%%%%%%%%%%%%%%%%%%%%%%%%%%%%%%%%%%%%%%

observed=data.T2;

plotx=40:0.01:100;
values=Fits_T2(plotx);
plot(plotx,values)

[m,n]=size(data.o2_measured);

for i=1:m
idx=find(plotx == data.o2_measured(i,n));
expected(i,1)=values(idx);

end

[row,col]=size(expected);
chi=0;

for i=1:row

chi=((observed(i,1)-expected(i,1))^2/expected(i,1))+chi;
end

dof=row-1;
alpha=0.05;
chi

%If chi calculated > chi square critical-->reject H0
%Very unlikely that the distribution is true.
```

C Paired t-test for SE and BOLD sequences

P value and statistical significance:
Two-tailed P-value=0.0763.

Confidence interval:
The mean of BOLD minus SE equals 21.60.
95% confidence interval: From -3.64 to 46.84

Intermediate values used in calculations:
t = 2.3758
df = 4
standard error of difference = 9.092

Group	BOLD	SE
Mean	175.2	153.6
SD	71.69	90.07
SEM	32.06	90.07
N	5	5

D Arduino code for solenoid valves control

```
1
2  #include <Wire.h>
3  #include <LCD.h>
4  #include <LiquidCrystal_I2C.h>
5  #include <avr/io.h>
6  LiquidCrystal_I2C lcd(0x3F,2,1,0,4,5,6,7);
7  // 0x3F is the I2C bus address  SDA->A4, SCL->A5
8
9  float bpm = 10.0,
10 heart_period = 1000.0,
11 heart_freq = 1.0,
12 analog_value = 0;
13
14 void setup() {
15
16 pinMode(13,OUTPUT); //valve 1
17 pinMode(12,OUTPUT); // valve 2
18 pinMode(11,OUTPUT); // trigger (same as valve 1)
19 lcd.begin (16,4);
20 lcd.setBacklightPin(3,POSITIVE);
21 lcd.setBacklight(HIGH);
22 Serial.begin(9600);
23 }
24
25 void loop() {
26
27 analog_value = analogRead(A3);
28 bpm = 60+analog_value/1023*180 ;
29 heart_period = 60/bpm *1000;
30 Serial.println(analog_value);
31
32 // Initial Phase
33
34 if (analog_value<50) {
35
36 // initial  Phase
37 digitalWrite(13, HIGH);
38 digitalWrite(12,HIGH);
39 digitalWrite(11,HIGH);
40
41 lcd.clear();
42 lcd.home();
43 lcd.print("*  Initial Phase.  *");
```

```
44
45 }
46
47 // 4 states
48 if (analog_value>70)
49 {
50
51 // state 1
52 digitalWrite(13, HIGH);
53 digitalWrite(12, LOW);
54 digitalWrite(11, HIGH);
55 delay(1.7*heart_period/4);
56
57 // state 2
58 digitalWrite(13, LOW);
59 digitalWrite(12, LOW);
60 digitalWrite(11, LOW);
61 delay(heart_period/8);
62
63 // state 3
64 digitalWrite(13, LOW);
65 digitalWrite(12, HIGH);
66 digitalWrite(11, LOW);
67 delay(1.3*heart_period/4);
68
69 // state 4
70 digitalWrite(13, LOW);
71 digitalWrite(12, LOW);
72 digitalWrite(11, LOW);
73
74 delay(heart_period/8);
75
76 display_bpm(bpm);
77 }
78 }
79
80 void display_bpm(long bpm)
81 {
82 lcd.clear();
83 lcd.home();
84 lcd.print("*  Heartphantom.  *");
85 lcd.setCursor(0,1);
86 lcd.print("BPM :");
87 lcd.print(bpm,1);
88 }
```

E Signal Intensities Paramagnetic Solution

TE (ms)	Sample 1	Sample 2	Sample 3	Sample 4	Sample 5	Sample 6
10	1338	1206	1357	1384	1223	1191
50	1993	1291	1375	1253	1039	830
100	1849	932	965	786	630	422
150	1738	718	708	536	412	277

F Signal Intensities Adult Test

F.1 Calibration Adult 2 samples

TE (ms)	Sample 1	Sample 2	Sample 3	Sample 4	Sample 5
10	830	872	729	505	493
50	803	715	427	166	108
100	475	253	216	70	73
150	289	134	177	88	61

F.2 Calibration Adult 3 samples

TE (ms)	Sample 1	Sample 2	Sample 3	Sample 4	Sample 5
10	864	857	890	929	831
50	827	811	727	398	205
100	485	435	278	125	127
150	298	250	140	128	119

F.3 Validation Adult Heart in-vivo

TE (ms)	Right Ventricle	Left Ventricle
10	1386	1493
50	511	928
100	176	510
150	85	113

*NOTE: Signal Intensities for Adult 1 where not used due to excess noise in the images.

G Signal Intensities Fetal Test

G.1 Calibration Fetal 1 samples

TE (ms)	Sample 1	Sample 2	Sample 3	Sample 4	Sample 5	Sample 6
10	866	936	1025	1024	1056	814
50	743	726	760	531	388	236
100	435	401	379	200	161	157
150	286	236	217	144	126	145

G.2 Calibration Fetal 2 samples

TE (ms)	Sample 1	Sample 2	Sample 3	Sample 4	Sample 5
10	802	838	811	881	831
50	725	656	309	263	230
100	391	366	125	144	121
150	236	198	100	136	125

G.3 Validation Fetal Heart in-vivo

TE (ms)	Left Ventricle
10	803
50	367
100	192
150	60

List of Figures

List of Tables

References

[1] Brian G Barratt-Boyes and Earl H Wood. The oxygen saturation of blood in the venae cavae, right-heart chambers, and pulmonary vessels of healthy subjects. *The Journal of Laboratory and Clinical Medicine*, 50(1):93–106, aug 2017.

[2] Matt Bernstein and Kevin King. *Handbook of MRI Pulse sequences*. Elsevier, iii edition, 2004.

[3] UT Block. Suppresion of MRI truncation artifacts using total variation constrained data extrapolation. *Int J Biomed Imaging*, Article ID, 2008.

[4] William Bradley. MR Appearance of Hemorrhage in the Brain. *Radiology*, 189(1):15–26, 1993.

[5] K BrielySabo. Accurate de-oxygenation of ex vivo whole blood using sodium dithionite. *Proc. Intl. Sot. Mag. Reson. Med*, 117(1985):2025, 2000.

[6] Richard Buxton. Dynamics of blood flow and oxygenation changes during brain activation: the balloon model. *US National Library of Medicine*, 39(6):855–64, 1998.

[7] Richard Buxton. Relaxation and contrast in MRI. In *Introduction to Functional Magnetic Resonance Imaging: Principles and Techniques*, chapter 1, page 930. Cambridge University Press, 2009.

[8] Richard B. Buxton and Lawrence R. Frank. A model for the coupling between cerebral blood flow and oxygen metabolism during neural stimulation. *Journal of Cerebral Blood Flow & Metabolism*, 17(1):64–72, 1997. PMID: 8978388.

[9] Mark S Cartier. The normal diameter of the feta aorta and pulmonary artery: Electrocardiograph evaluation in utero. *PubMed*, 5(151):991–3, 1988.

[10] Catie Chang, John P. Cunningham, and Gary H. Glover. Influence of heart rate on the BOLD signal: The cardiac response function. *NeuroImage*, 44(3):857–869, feb 2009.

[11] GB Chavhan. Steady-State MR Imaging Sequences: Physics, Classification, and Clinical Applications. *RadioGraphics*, 28(4), 2008.

[12] LF Czervionke. Characteristic features of MR truncation artifacts. *AJR am J Roetgenol*, 151:1219:1228, 1988.

[13] Patricia A. Dunn, Stuart Weiner, and Avi Ludomirski. Percutaneous umbilical blood sampling. *Journal of Obstetric, Gynecologic and Neonatal Nursing*, 17(5):308 – 313, 1988.

[14] George Eastman and Christoph Wald. *Getting Started in Clinical Radiology*. Thieme, 2011.

[15] Matthias G. Friedrich and Theodoros D. Karamitsos. Oxygenation-sensitive cardiovascular magnetic resonance. *Journal of Cardiovascular Magnetic Resonance*, 15(1):43, 2013.

[16] Akash Ganguly. Larmor frequency and spin orientation. In *Nuclear Magnetic Resonance and MRI*, chapter 1, page 124. Academic Publishers, 1 edition, 2016.

[17] John M. Gomori. NMR Relaxation Times of Blood: Dependence of Field Strength, Oxidation State, and Cell Integrity. *Journal of Computer Assisted Tomography*, 11(4):684–690, 1987.

[18] Carol Green. *Primary Care Pediatrics*. Lippincott, 2001.

[19] E. L. Hahn. Spin echoes. *Phys. Rev.*, 80:580–594, Nov 1950.

[20] Ronald B Hirschl, Palle Palmer, Kurt F Heiss, Karl Hultquist, Franco Fazzalari, and Robert H Bartlett. Evaluation of the right atrial venous oxygen saturation as a physiologic monitor in a neonatal model. *Journal of Pediatric Surgery*, 28(7):901–905, aug 2017.

[21] Joseph Hornak. *The basics of MRI*. Rochester Institute of Technology, New York, xvii edition, 2017.

[22] D Hutter, J Kingdom, and E Jaeggi. Causes and mechanisms of intrauterine hypoxia and its impact on the fetal cardiovascular system: a review. *Int J Pediatr*, 2010:401323, 2010.

[23] S. Kim. Comparison of blood oxygenation and cerebral blood flow effects in fMRI: estimation of relative oxygen consumption change. *US National Library of Medicine*, 38(2):59–65, 1997.

[24] Peiying Liu, Lina F. Chalak, Lisa C. Krishnamurthy, Imran Mir, Shin Lei Peng, Hao Huang, and Hanzhang Lu. T1 and T2 values of human neonatal blood at 3 Tesla: Dependence on hematocrit, oxygenation, and temperature. *Magnetic Resonance in Medicine*, 75(4):1730–1735, 2016.

[25] H. Lu. Quantitative evaluation of oxygenation in venous vessels using T2-Relaxation-Under-Spin-Tagging MRI. *Magnetic Resonance in Medicine*, 60:357–363, 2008.

[26] Hanzhang Lu, Feng Xu, Ksenija Grgac, Peiying Liu, Qin Qin, and Peter Van Zijl. Calibration and validation of TRUST MRI for the estimation of cerebral blood oxygenation. *Magnetic Resonance in Medicine*, 67(1):42–49, 2012.

[27] Arumana Mangalathu, Debiao Li, and Rohan Dharmakumar. Deriving Blood-Oxygen-Level-Dependent Contrast in MRI with T*2 Weighted, T2-prepared and phase-cycled SSFP methods: Theory and Experiment. *Magnetic Resonance in Medicine*, 59(3):561–570, 2009.

[28] Robert Manka, Ingo Paetsch, Bernhard Schnackenburg, Rolf Gebker, Eckart Fleck, and Cosima Jahnke. Bold cardiovascular magnetic resonance at 3.0 tesla in myocardial ischemia. *Journal of Cardiovascular Magnetic Resonance*, 12(1):54, 2010.

[29] Peter John Murphy. The fetal circulation. *Continuing Education in Anaesthesia Critical Care and Pain*, 5(4):107, 2005.

[30] Renate Oberhoffer, Josef Högel, and Dieter Lang. Normal characteristics of cardiac dimensions and function in the fetus. *European Journal of Ultrasond*, 2:93–106, 1995.

[31] S. Ogawa and T. Lee. Magnetic resonance imaging of blood vessels at high fields: in vivo and in vitro measurements and image simulation. *Magnetic Resonance Medicine*, 16(1):9–18, 1990.

[32] Linus Pauling and Charles Coryell. The Magnetic Properties and Structure of Hemoglobin, Oxyhemoglobin and Carbonmonoxyhemoglobin. *Proceedings of the National Academy of Sciences of the United States od America*, 22(4):210–216, 1936.

[33] L. Peiying. T1 and T2 Values of Human Neonatal Blood at 3 Tesla: Dependence on Hematocrit, Oxygenation, and Temperature. *Magnetic Resonance in Medicine*, 1(50):230–236, 2015.

[34] Martin Ramon. *Anesthetic and Obstetric Management of High Risk Pregnancy.* Springer, 18 edition, 2004.

[35] Peter Reimer, Paul Parizel, and James Meany. Principles of Magnetic Resonance. In *Clinical MR Imaging*, chapter 1, page 820. Springer Science and Business Media, 2010.

[36] John Ridgway. Cardiovascular magnetic resonance physics for clinicians. *Journal of Cardiovascular Magnetic Resonance*, 12(1):71, 2010.

[37] L. D. Schearer and G. K. Walters. Nuclear spin lattice relaxation in the presence of magnetic-field gradients. *Phys. Rev.*, 139:A1398–A1402, Aug 1965.

[38] Klaus Scheffler. Is TrueFISP a gradient-echo or a spin-echo sequence? *Magnetic Resonance in Medicine*, 49(2):395–397, 2003.

[39] John Schenck. The role of magnetic susceptibility in magnetic resonance imaging: MRI magnetic compatibility of the first and second kinds. *Medical Physics*, 23(6):816–850, 1996.

[40] Abhishek Sharma. Blood oxygen level-dependent magnetic resonance imaging in patients with coronary artery disease. *Journal of the American College of Cardiology*, 60(18):1842–1843, 2012.

[41] M. J. Silvennoinen, C. S. Clingman, X. Golay, R. A. Kauppinen, and Peter C M Van Zijl. Comparison of the dependence of blood R2 and R2* on oxygen saturation at 1.5 and 4.7 Tesla. *Magnetic Resonance in Medicine*, 49(1):47–60, 2003.

[42] Robert Simioni and Martha Aughan. The Structure and Function of Hemoglobin. In The American society for Biochemisrty and Molecular Biology, editor, *The Hemoglobin System*, volume VI, pages 529–545. Adair, 1998.

[43] Celeste Simon. The role of oxygen availability in embryonic development and stem cell function. *PubMed*, (9):285–296, 2008.

[44] Emine Ulku Saritas Thangavel, Kalaivani. Aqueous paramagnetic solutions for MRI phantoms at 3T A detailed study on relaxivities. *National Magnetic Resonance Reacher Center*, 2016(17):1–6, 2016.

[45] Loren Thompson, Sarah Crimmins, Bhanu Telugu, and Shifa Turan. Intrauterine hypoxia: clinical consequences and therapeutic perspectives. *Research and Reports in Neonatology*, Volume 5:79, sep 2015.

[46] Keith R. Thulborn, John C. Waterton, Paul M. Matthews, and George K. Radda. Oxygenation dependence of the transverse relaxation time of water protons in whole blood at high field. *BBA - General Subjects*, 714(2):265–270, 1982.

[47] Robert-Jan M. van Geuns, Piotr A. Wielopolski, Hein G. de Bruin, Benno J. Rensing, Peter M.A. van Ooijen, Marc Hulshoff, Matthijs Oudkerk, and Pim J. de Feyter. Basic principles of magnetic resonance imaging. *Progress in Cardiovascular Diseases*, 42(2):149–156, sep 1999.

[48] Peter van Zijil. Quantitative assessment of blood flow, blood volume and blood oxygenation effects in functional magnetic resonance imaging. *Nature medicine*, 4(1):159 – 167, 1998.

[49] Ulrike Wedegaertner, Hendrik Kooijman, Jin Yamamura, Michael Frisch, Christoph Weber, Ralph Buchert, Anna Huff, Kurt Hecher, and Gerhard Adam. In vivo MRI measurement of fetal blood oxygen saturation in cardiac ventricles of fetal sheep: A feasibility study. *Magnetic Resonance in Medicine*, 64(1):32–41, 2010.

[50] G. Wesbey, M. Moseley, and R. Ehman. Translational molecular self-diffusion in magnetic resonance imaging: effects and applications. *Biomedical magnetic resonance*, University:63–76, 1984.

[51] John Wiley and Mark Brown. *MRI Basic principles and Applications.* V edition, 2015.

[52] Robert Woods. Long-term trends in fetal mortality: implications for developing countries. *Bulletin of the World Health Organization*, 86:417–496, 2008.

[53] Jason M. Zhao, Chekesha S. Clingman, M. Johanna Närväinen, Risto A. Kauppinen, and Peter C M Van Zijl. Oxygenation and hematocrit dependence of transverse relaxation rates of blood at 3T. *Magnetic Resonance in Medicine*, 58(3):592–597, 2007.